IMMUNOFLUORESCENCE DETECTION OF QUANTUM DOT LABELED CANCER CELLS

MICROCONTACT PRINTING, NANOPOROUS SURFACE ENHANCED ABSORPTION, AND MICROFLUIDIC APPLICATIONS

Elaine Ng

BME 679HB
Special Honors in the Department of Biomedical Engineering
The University of Texas at Austin

May 2013

IMMUNOFLUORESCENCE DETECTION OF QUANTUM DOT LABELED CANCER CELLS

MICROCONTACT PRINTING, NANOPOROUS SURFACE ENHANCED ABSORPTION, AND MICROFLUIDIC APPLICATIONS

Elaine Ng

BME 679HB
Special Honors in the Department of Biomedical Engineering
The University of Texas at Austin

May 2013

Dr. John X.J. Zhang
Department of Biomedical Engineering
Supervising Professor

Dr. Jeanne Stachowiak
Department of Biomedical Engineering
Second Reader

Immunofluorescence Detection of Quantum Dot Labeled Cancer Cells: Microcontact Printing, Nanoporous Surface Enhanced Absorption, and Microfluidic Applications

Elaine Ng

Biomedical Engineering, B.S.

The University of Texas at Austin, 2013

Supervisor: Dr. John X.J. Zhang

Detection of circulating tumor cells (CTCs) in blood has been rapidly developing into a promising early cancer diagnostic tool. CTCs provide crucial evidence of the progression and status of the disease. Early cancer detection provides a powerful prevention step, allowing for effective treatment. This thesis presents an efficient method for cancer cell capture via cell line-specific antibody deposition and adsorption on nanoporous silica substrates using a method called “micro-contact printing” and immunofluorescence detection through quantum dot labeling within a microfluidic system.

Microcontact printing is essential in efficient design, characterization, and production of biologics for cost effective, high throughput, and point-of-care detection and analysis system. Nanoporous silica enhances the adsorption of proteins onto its surface. Quantum dots enable brighter and more stable fluorescence imaging of biological species. Additionally, microfluidic systems allow for more effective antibody-antigen interactions due to physical dimensional constraints of the microfluidic channel itself, forcing closer proximities between antigen and

antibody, thus increasing binding probabilities. Coupled together, a compact system for efficient and effective microchip-based diagnostics and detection can be designed.

Such a system sets the stage for a versatile platform capable of single cell based analyses including manipulation, sensing and imaging for different biomedical applications. Within a single biosensing platform, it integrates multiple functions such as multiplexing and multicolor detection capabilities. Each component of the platform plays an important role in enhancing the sensitivity and specificity. The proposed research shows great promise for potential applications in high throughput screening and drug assays, cellular biomarker studies, site-specific cell culturing in microarrays and cancer cell detection.

Acknowledgements

I am extremely grateful to have Dr. John X.J. Zhang as my undergraduate advisor and supervisor. He has been incredibly supportive and encouraging during my undergraduate research career. He provided the structure and guidance that has influenced and shaped me into the innovative and open-minded researcher I am today. I appreciate the training he has given me to prepare me well for graduate school as well as the opportunities he has given me to pursue and achieve more than the average undergraduate researcher can achieve working in a lab. These last four years of being a part of his lab has helped built both my independence and confidence in scientific research.

I would also like to thank Dr. Kazunori Hoshino for being an extremely helpful and wonderful mentor in lab. Many of my technical skills and experimental protocols were learned and derived through discussions with him. He has also been supportive in my research pursuits and a major influence in my research.

I would like to thank all the members of the Zhang Lab for providing me with such an inspiring and comfortable environment. Without them, my undergraduate research experience would not have been as lively and enjoyable as it was. Time and time again, they have helped motivate me and taught me the technical skills I needed to be successful in conducting my experiments.

Lastly, I thank my family, especially my mom and dad, for their support throughout my life. They are truly the pillars that hold me up during times of difficulty. Their advice and motivation has been and will always be a monumental impact in my life. Without them, I would not be who I am today.

Table of Contents

Abstract i

Acknowledgements iii

Table of Contents iv

List of Figures vii

List of Tables ix

1 Introduction 1

1.1 Background and Motivation 1

1.1.1 Cancer Metastasis 1

1.1.2 Early Diagnostics and Detection 2

1.2 Thesis Organization 5

2 Microcontact Printing on Nanoporous Silica Substrate 7

2.1 Nanoporous Silica Thin Film Substrates 7

2.1.1 Fabrication of Porous Silica Substrates 9

2.2 Microcontact Printing 10

2.2.1 Multicolor Microcontact Printing 11

2.2.2 Optical Observations of Multicolor Protein Patterning 13

2.2.3 AFM Characterization of Printed Protein Layers 14

2.3 Patterned Sandwich Enzyme Linked Immunosorbent Assay 16

2.3.1 Protein Sample Extraction 17

2.3.2 Microcontact Printed Sandwich ELISA 17

2.3.3 Results and Discussion 19

2.4 Conclusion 20

3 Quantum Dots as Contrast Agents 22
4 Fundamentals of Microfluidic Channels 28
5 Patterned ELISA Cancer Cell Detection 34
5.1 Experimental Methods 34
5.1.1 Cell Culture 34
5.1.2 Microcontact Printing of Capture Antibody 35
5.1.3 Immunofluorescence Detection of QD Labeled Cancer Cells 37
5.1.4 Statistical Analysis 38
5.2 Results and Discussion 40
5.2.1 Characterization of Printed Capture Antibody 40
5.2.2 Immunofluorescence Detection of QD Labeled Cancer Cells 41
5.2.3 Statistical Analysis: Cancer Cell Capture Numbers 43
5.3 Conclusion 46
6 Site-Specific Cancer Cell Detection in Microfluidics 47
6.1 Experimental Methods 47
6.1.1 Microfluidic Modeling 47
6.1.2 Site-Specific Cancer Cell Capture 48
6.1.3 Statistical Analysis 50
6.2 Results and Discussion 50
6.2.1 Modeling of the Microchannel 50
6.2.2 Microfluidic Integration 52
6.3 Conclusion 54
7 Closing Remarks and Future Directions 55

8 References 56

List of Figures

Figure 1. Proposed CTC Detection System 4

Figure 2. Typical IgG Antibody 8

Figure 3. Nanoporous Silica Substrate Fabrication 9

Figure 4. Microcontact Printing 11

Figure 5. Microcontact Printing Apparatus 11

Figure 6. Multicolor Multiple Microcontact Printing 12

Figure 7. Multicolor Immunofluorescence Detection of Proteins 14

Figure 8. Quantification of Printed Protein Layers 15

Figure 9. Micropatterned ELISA 18

Figure 10. Fluorescence Imaging of Micropatterned Sandwich ELISA 20

Figure 11. Synthesized Colloidal QDs 23

Figure 12. Detection of HER2 with QD-IgG 24

Figure 13. HMI Cancer Cell Imaging 26

Figure 14. Integrated Bioimaging System 27

Figure 16. Flow Profiles within a Tube 29

Figure 15. Soft Lithographic Fabrication of Microfluidic Channels 29

Figure 17. Microchip-based Immunomagnetic Detection of Cancer Cells 30

Figure 18. CTC-Chip and HB-Chip 31

Figure 19. Lung-on-Chip 32

Figure 20. Microcontact Printing Process 36

Figure 21. Immunofluorescence Detection of QD-Labeled Cancer Cells 37

Figure 22. Characterization of Patterned Nanoporous Substrates 40

Figure 23. Cancer Cell Imaging 42

Figure 24. Model Microfluidic Channel 48

Figure 25. Site Specific Capture 49

Figure 26. Microchannel Modeling 51

Figure 27. Capture Site-Specific Cancer Cell Imaging 53

List of Tables

Table 1. Thickness and roughness measurements of printed proteins. 15

Table 2. Average captured cell numbers within the defined 1 cm x 1 cm nanoporous silica square area and respective standard deviations obtained from each of the six different experimental conditions. 43

Table 3. Comparisons of all group-by-group p-values**.** 44

1 Introduction

1.1 Background and Motivation

1.1.1 Cancer Metastasis

Cancer is a condition in which the body experiences uncontrolled growth of abnormal cells. Cancer cells originate from normal cells in the body that hyperactively divide at a rapid rate due to genetic mutations in the cells' deoxyribonucleic acid (DNA) [1]. Many different types of cancer exist and can be caused or triggered by various genetic or environmental factors, such as tobacco smoking, diet and physical activity, and sun or UV exposure [2]. As one of the leading causes of death, cancer is the cause of about 13% of all deaths in 2008 [3].

One of the primary reasons why cancer has been deemed such a malignant and potent disease is due to its ability to spread to other parts of the body and become metastatic. Circulating tumor cells (CTCs) are tumor cells that have detached from the primary tumor site and are circulating in the patient's peripheral circulatory system or lymphatic system [4]. CTCs travel to and lodge themselves at secondary tumor sites. There, they remain dormant until triggered by specific complex cellular signals, wherein they begin to metastasize, growing and developing into a secondary cancerous tumor.

Therefore, it has become exceedingly important to be capable of detecting and diagnosing the disease in its early stages before further metastasis and deterioration of patient health occur. Early cancer diagnostics is the most powerful prevention step, preventing spread of the disease beyond the already affected area by allowing for earlier and easier treatment. It also provides the motivation behind the cancer detection system presented in this thesis.

1.1.2 Early Diagnostics and Detection

Conventional detection and diagnosis of cancer includes tumor biopsy, bone marrow biopsy, computed tomography (CT) scans, and magnetic resonance imaging (MRI) scans. These common methods of detection each have their drawbacks. Biopsies are invasive and usually require the patient to undergo surgery, while CT scans use ionizing radiation, thus subjecting the patient to radiological health risks. Although MRI scans are generally less invasive, they introduce additional hassles for the patient. MRI relies on magnetic fields which can affect any magnetically susceptible metal. Metallic implants in patients, such as aneurysm clips, cardiac pacemakers, or insulin pumps may be damaged or shifted during an MRI scan. Additionally, these methods of detection are expensive and usually only capable of providing accurate detection and diagnostics information when the patient is in later stages of cancer. Whereas conventional cancer detection methods involve invasive procedures and is mostly conducted at the macroscopic tissue level, the proposed device seeks to detect cancer metastasis and progress at a cellular level in a minimally invasive way.

Due to the drawbacks in conventional detection and diagnostic methods, much research has been dedicated to other methods. Development of devices embodying characteristics of point-of-care systems, including low cost, highly mobile, and miniaturization, has been favored and advantageous. The small amounts of reagents and samples required by these point-of-care devices have the potential to greatly reduce the cost of a single test, as well as promoting patient compliance. Miniaturization of the devices enables samples to be easily transferred from place to place when needed, increasing convenience and efficiency for both medical doctors and clinical patients.

Recent developments in point-of-care detection systems have strongly emphasized and concentrated on the capture and detection of CTCs as early indications of cancer by means of

biomarker assessment. The presence of CTCs may also provide information about a patient's current disease state [5]. However, devices developed for the purpose of capturing and detecting CTCs must be both sensitive as well as specific given the fact that CTCs are extremely rare. CTC counts can be as low as one CTC per 10^6 – 10^7 leukocytes [4]. Additionally, the presence of several various types and subtypes of biomarkers on the surface of the CTC during different stages of the cellular growth makes it difficult for enumerating and detecting CTCs in a consistent manner [4, 6, 7]. Hence, several studies have been dedicated to finding specific biomarkers that are typically overexpressed and can effectively distinguish CTCs from other cells of the body. Some commonly known biomarkers include prostate-specific antigen (PSA) for detection of prostate cancer [6] and human epidermal growth factor receptor 2 (HER2) for breast cancer [8].

A prime example of a developing early diagnostic point-of-care system that utilizes biomarker detection of CTCs is the CellSearch® CTC Test from Veridex, LLC, a subsidiary company of Johnson & Johnson. CellSearch® is designed as a blood test capable of helping doctors predict disease state and provide a relatively accurate prognosis for patients with metastatic breast, colorectal, or prostate cancer based on the number of CTCs found within a tube of blood [9]. The system captures and detects CTCs through the use of epithelial cell adhesion molecule (EpCAM) coated magnetic nanoparticles which bind to CTCs in the patient blood sample [10].

Although the CellSearch® CTC Test has been approved and cleared for marketing by FDA, and has made considerable advancement in cancer diagnostics and detection, it still has its limitations. For one, a system solely reliant on a single biomarker may be questionable in terms of its sensitivity due to the versatile nature of cellular biomarker expression depending on the

individual cell and the stage of growth [11, 12]. The system is also limited in terms of its capability for post cell analysis, assessment, and imaging. Since it is a liquid based test, cells remain suspended in blood sample during capture and immunofluorescence analysis, after which the sample is discarded, along with the CTCs.

The detection system presented in this thesis aims to address the previously stated issues concerning capture and detection of CTCs, as well as introduce design aspects to enhance the capturing, imaging, and analysis process. The proposed system, shown in **Figure 1**, consists of three primary components: a microcontact printed nanoporous silica substrate for enhanced protein absorption and deposition, a microfluidic channel for closer interaction between antibodies and cells and high throughput capability, and quantum dots (QDs) for effective and stable imaging of cells with potential for simultaneous multicolor detection.

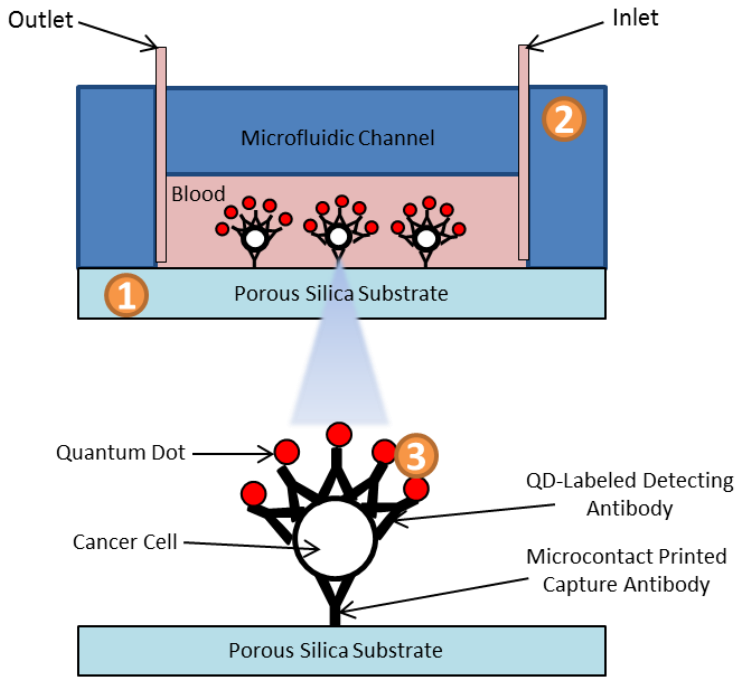

Figure 1. Proposed CTC Detection System. *The device consists of three major components: 1) a microcontact printed nanoporous silica substrate, 2) a microfluidic channel, and 3) quantum dots.*

Ultimately, when integrated together, the three components will produce a low cost, high throughput, miniaturized point-of-care device designed for the capture, detection, imaging, and analysis of CTCs in patient blood samples.

1.2 Thesis Organization

This thesis documents the development of microchips that combines the advantages of micro and nanotechnologies to create effective and efficient platforms for various biological applications. In particular, the microchips make use of 1) microcontact printing, 2) nanoporous silica substrates, 3) quantum dots, and 4) microfluidic channels. The feasibility of the combination of such technologies was demonstrated in the performance of high throughput enzyme linked immunosorbent assays for food allergen detection and multicolor micropatterning. Ultimately, the most important and the primary focus of the thesis is designing a microchip-based platform that combines the advantages of the technologies for the purpose of effective and efficient capturing, imaging, and analysis of cancer cells.

The first part of the thesis focuses on introducing the micro and nanotechnologies and techniques of particular interest and utilized in the final microchip platform. This part introduces the effectiveness of the combination of the microcontact printing (μCP) technique on a nanoporous silica substrate in protein detection for multicolor patterning and immunoassays. The concept behind the use of the μCP technique involves simple uniform monolayer deposition and transfer of proteins that also enables potential multiplexing of multiple antibodies on a single substrate for selective and specific multiple antigen detection. Incorporation of the nanoporous silica substrate involves enhanced protein and antibody absorption that allow for more effective and efficient detection. In addition, quantum dots will be introduced to emphasize the benefits of QD immunofluorescence labeling of cancer cells. The use of QDs for immunofluorescence

labeling of cancer cells involves the capability for brighter, more stable, and potentially simultaneous multicolor imaging. Finally, microchannels will be introduced to form the final microchip-based platform for cancer cell capture and detection. The concept behind the use of a microfluidic channel involves finding optimal microchannel dimensions and geometries, as well as optimal flow conditions, for enhanced antibody and cancer cell interaction and binding.

The second part of the thesis focuses on demonstrating the application of the technologies described in the first half. In particular, demonstration of proof of concept of the static capturing of cancer cells and site-specific targeted cancer cell capture using a microchip platform that derives its working principles from the advantages of the μCP technique and nanoporous silica. This part also emphasizes the benefits of QD immunofluorescence labeling of cancer cells. To complete the platform, a study of the effects of integrating the previously mentioned components with a geometrically-defined grooved microfluidic channel, thus converting the system to a dynamic system by introducing flow is demonstrated. This last part illustrates the enhanced effect on the capture numbers of cancer cells in the dynamic microfluidic system with the capture numbers of cancer cells in the static system introduced earlier.

Finally, the thesis concludes with an introduction of future applications and prospects for the utilization of the cancer cell capturing microchip. In general, typical immunoassays require long procedures that involve the use of microliter well plates and generous amounts of reagents, and quantification using spectrophotometry. Miniaturization of such systems onto a single microchip, allows for a low cost and high throughput device, both key characteristics of point-of-care devices. More interestingly, as shown in this thesis, the fundamental working principles of the microchips have potential to be applied across various biological applications.

2 Microcontact Printing on Nanoporous Silica Substrate

This section of the thesis introduces the advantages of the µCP technique coupled with nanoporous silica substrates. These two micro and nanotechnologies are integrated to demonstrate its advantage in enhancing the detection of proteins of interest. These fundamental working principles can be expanded to provide an attractive system for various biological detection systems or biosensors as described later.

2.1 Nanoporous Silica Thin Film Substrates

Conventional methods of surface functionalization involve chemical modifications in order to either increase or decrease substrate affinity for particular proteins, depending on the specific application [13–16]. Chemical modifications of surfaces to increase protein affinity usually involve the use of silane compounds that have terminal functional groups that can interact electrostatically or covalently with protein surface groups. Although chemical modification has been shown to yield effective results in increasing protein absorption, the processes involved are normally intricate and detailed in nature. Physical surface modifications, such as creating porous thin film structures for deposition on a substrate surface, are relatively straightforward approaches to surface modification. Nanoporous thin film characteristics are also easy to manipulate by changing fabrication conditions.

The physical structures of the porous thin film allow for size-selective trapping of proteins and thereby enhancing protein absorption [17–20]. It has been previously shown by Blinka et al., that nanoporous silica thin film functionalized substrates enhance protein adhesion and adsorption onto the substrate surface more so than surfaces functionalized by chemicals such as 3-aminopropyltriethoxysilane (APTES) and glutaraldehyde (GA). Additionally, upon

comparison of nanoporous silica substrates with varying pore sizes, thin film thicknesses, and porosities, it was shown that nanoporous silica substrates characterized by 4 nm pores, 30 – 100 nm thin film thickness, and 57% porosity were most effective in protein absorption [17]. By using nanoporous silica thin film substrates for enhanced protein absorption, it can be ascertained that the microcontact printed capture antibody is effectively transferred and absorbed onto the microchip substrate surface.

Here, a nanoporous silica thin film of about 100 nm in thickness, with 4 nm pores and a porosity of 57%, is deposited on silicon substrate to form the base of the detection system. The µCP technique, described later, is employed in the deposition and transfer of the capture antibody onto the nanoporous silica substrate surface. The resulting stamped samples are characterized to verify the formation of an antibody self-assembled monolayer (SAM) and uniformity of the stamped antibody layer. Because immunoglobin G (IgG) antibodies have typical dimensions of 8.5 nm x 14.4 nm x 4 nm [21] (see **Figure 2**), the 4 nm pores of the porous silica thin film assist in anchoring and securing antibodies in place on the substrate, aligning them so that the epitopes are optimally exposed to antigens for binding. Additionally, the porous nature of the thin film increases the surface area of substrate area which comes into contact with the µCP stamp, and thus increases the capture antibody density per unit area. The increase in antibody density enhances the sensitivity of the microchip, a critical aspect of detection

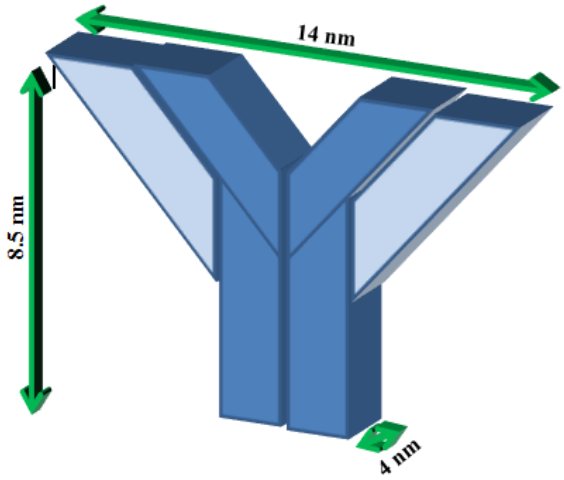

Figure 2. Typical IgG Antibody. *A typical IgG antibody has the dimensions of 8.5 x 14.4 x 4 nm.*

systems and ultimately, the goal of the proposed detection microchip presented in this thesis.

2.1.1 Fabrication of Porous Silica Substrates

The nanoporous silica thin film substrates were fabricated according to the conditions and methods described by Blinka et al. [17] for substrates with 4 nm pore sizes, 130 $\pm$ 0.5 nm thickness, and 52.4 $\pm$ 0.2% porosity. In summary, surfactant micelles were formed by self-assembly between polymer units and mixed with soluble silicates, tetraethyl orthosilicate (TEOS) and tetraethoxysilane, in homogeneous, hydro-alcoholic solutions. As the solvent evaporates during spin coating, the increase in polymer concentration causes the solution to exceed critical micelle concentration, driving silica/copolymer self-assembly into a uniform thin-film nanophase.

TEOS was dissolved in a mixture of ethanol (EtOH), distilled water (diH_2O), and hydrochloric acid (HCl) and stirred for 2 hr at 75 ^oC to form a clear silicate solution. Pluronic F127, a triblock copolymer (PEO_{106}–PPO_{70}–PEO_{106}), was dissolved in EtOH and stirred at room temperature. The silicate solution was mixed into the F127-EtOH solution and stirred for 2 hr at room temperature. The resulting solution was deposited onto a silicon wafer by spin coating at a spin rate of 1500 rpm for 20 s, and then heated at 80 ^oC for 12 hr. The films were calcinated at 425 ^oC for 5 hr. to remove the organic surfactant. The nanoporous silica substrate surface was then oxygen plasma treated with an oxygen flow rate of 80 sccm and a power of 300

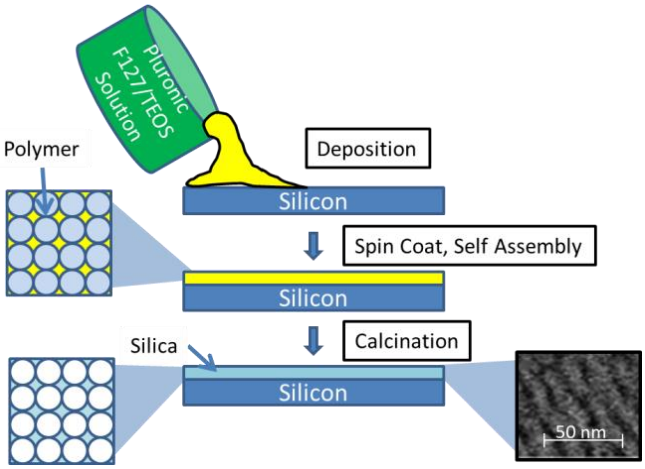

Figure 3. Nanoporous Silica Substrate Fabrication. *Schematic of the fabrication process of thin film nanoporous silica substrates [21]* **.**

W for 10 min. **Figure 3** shows the schematic of the fabrication of the nanoporous silica substrates.

The thickness of the thin film was controlled by adjusting the concentration of Pluronic F127. The porosity depends on the molar ratio of polymer and silicate in the starting material.

2.2 Microcontact Printing

Microcontact printing (μCP) was first introduced in 1993 by George M. Whitesides group as a method for producing self-assembled monolayers (SAMs) [22]. In contrast to conventional methods of creating SAMs, which involves an initial chemical modification of the substrate surface before molecules chemically bind to the surface, μCP involves simple physical contact between substrate and a stamp. Additionally, the technique provides greater convenience as well as flexibility due to its patterning capabilities. SAMs of various geometries and sizes ranging from micron to sub-micron features can be patterned [23]. Given its advantages over conventional methods of creating SAMs, μCP has been employed in a wide variety of applications, mostly in the fabrication of biosensors. It has been used in the patterning of proteins in immunoassays [17, 24–29], patterning of cells [29–32], and optical arrays [33–35]. μCP has provided an easy and simple method for quick surface functionalization with potential for multiplexing capabilities, a critical advantage when performing procedures such as immunoassays [15, 16].

The ability to pattern multiple proteins for multiplexing capability on a single substrate on a miniaturized scale is important in creating efficient point-of-care detection and analysis systems, which is the ultimate goal of the devices presented in this thesis.

2.2.1 Multicolor Microcontact Printing

Poly(dimethylsiloxane) (PDMS) stamps were fabricated from hard silicon masters [36] with 100 µm diameter by 20 µm high circular patterns and four corner alignment marks. The circular pattern on the two separate stamps of a set alternated so that when aligned correctly using the alignment marks, will form an alternating pattern (ABABAB). Stamps with pattern A were inked with a 5 µg mL^{-1} FITC-tagged (fluorescein isothiocyanate) anti-rabbit IgG (Sigma Aldrich) solution for 20 min. Stamps with pattern B were inked with a 5 µg mL^{-1} TRITC-tagged (tetramethyl rhodamine iso-thiocyanate) anti-rabbit IgG (Sigma Aldrich) solution for 20 min. Both stamps were washed with 0.01 M phosphate buffer saline solution (PBS) and de-ionized water (diH_2O) and dried under nitrogen (N_2) gas. **Figure 4** shows the basic schematic for µCP of a single protein onto nanoporous silica substrate. Stamp A and B were sequentially brought into contact with the nanoporous silica substrate for 1 min. Printing was done manually using a home-built stamping apparatus with a stamp-carrying part capable of micrometer level translations in the *x*, *y*, and *z* directions, to allow alignment precision within 5 µm (see **Figure 5**). In order to align the stamps and create a patterned substrate of the two different proteins, alignment markings on both stamps were aligned with corresponding alignment markings on the substrate. To visualize the alignment of

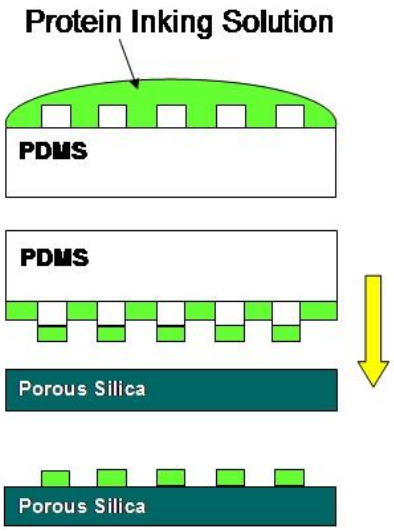

Figure 4. Microcontact Printing. *Schematic of the microcontact printing process.*

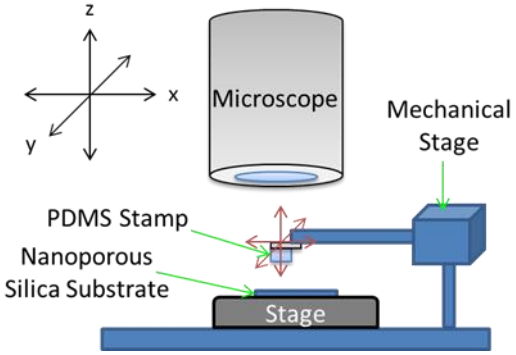

Figure 5. Microcontact Printing Apparatus. *Schematic of the µCP apparatus that allows for x, y, and z directional translations for precise alignment visualized using a microscope.*

the stamp with the substrate, a microscope with 5X was positioned above the apparatus. **Figure 6** shows the schematic for multiple microcontact printing. Transferred protein layers were analyzed by fluorescence (Olympus BX51) and atomic force microscopy (AFM; Digital Instruments Series IV, Veeco) for surface thickness and roughness to show uniform monolayer deposition of proteins.

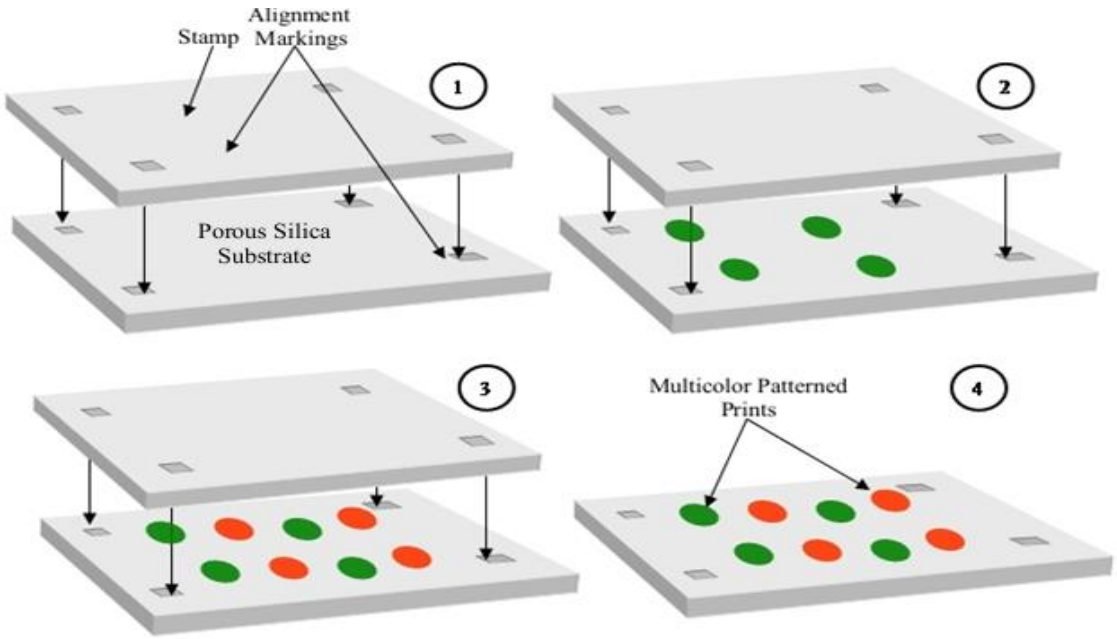

Figure 6. Multicolor Multiple Microcontact Printing. *Schematic of multiple microcontact printing. The alignment marks on the two stamps were aligned with corresponding alignment marks on the nanoporous silica substrate to ensure a patterning of the two different proteins*.

2.2.2 Optical Observations of Multicolor Protein Patterning

It was first demonstrated that two different proteins could be simultaneously microcontact printed onto a single substrate via careful manual alignment of a set of complementary stamps to the nanoporous silica substrate, facilitated by corresponding alignment markings on both stamps and substrate. The nanoporous silica substrate was put under a fluorescence microscope and excited under the FITC filter (excitation wavelength ~490 nm) and the TRITC filter (excitation wavelength ~557 nm). Both proteins fluoresced under their respective filters. Under the FITC filter, only the FITC rabbit IgG circular pattern showed positive green fluorescence, while TRITC rabbit IgG showed little to no fluorescence. Under the TRITC filter, only the TRITC rabbit IgG circular pattern showed positive red-orange fluorescence, while FITC rabbit IgG showed little to no fluorescence. This indicates successful transfer of the proteins and hence successful multicolor microcontact printing of two different proteins on the same substrate. **Figure 7** shows the resulting fluorescence microscopy pictures. As shown in the overlay, the alignment of the two stamps on the substrate was relatively precise, giving a small amount of displacement (about 30 μm). Because the stamping was manually performed and relative precision was eyeballed, there is large room for human error. Although 30 μm may seem small, on a nanoscale level, it is relatively large. Future improvements to the microcontact printing apparatus, perhaps even development of an automated apparatus, will potentially increase the precision and accuracy of alignment. However, such is beyond the scope of this thesis, and as shown by the overlay, a successful multicolor multicontact printing of two different proteins was demonstrated.

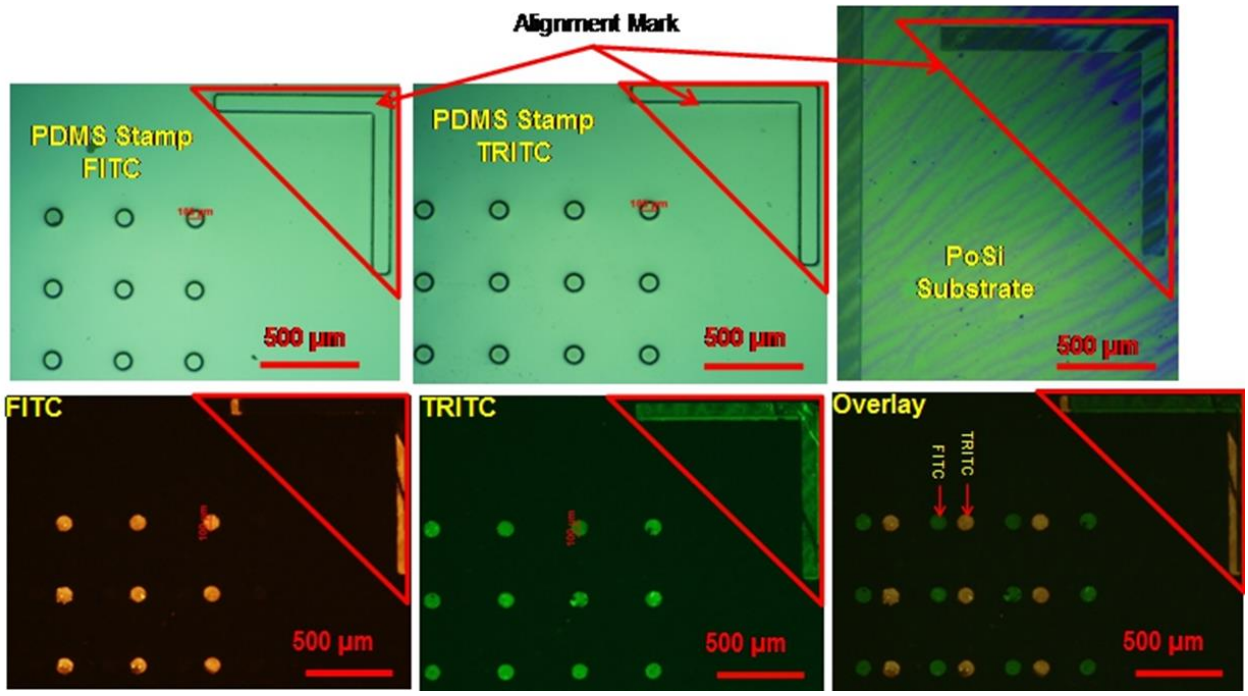

Figure 7. Multicolor Immunofluorescence Detection of Proteins. *(Top, left to right): PDMS stamp used to stamp FITC rabbit IgG antibodies; PDMS stamped used to stamp TRITC rabbit IgG antibodies; nanoporous silica substrate. All three have corresponding alignment markings to facilitate accurate stamping. (Bottom, left to right): Fluorescence microscopy pictures of substrate viewed under FITC filter; substrate under TRITC filters; overlay of the two pictures. The proteins on the substrate fluoresced under respective filters and the overlay demonstrates preciseness of alignment and no overlapping.*

2.2.3 AFM Characterization of Printed Protein Layers

The stamped protein layers were analyzed using AFM microscopy and Vernier LabPro to evaluate the consistency of the transfer of proteins from PDMS stamp to nanoporous silica substrate. Ten FITC protein circles and five TRITC protein circles were arbitrarily chosen on the substrate and evaluated for protein layer thickness and surface roughness. To calculate thickness data, AFM pictures were divided into regions of protein coverage and regions of background. 1 μm^2 areas were taken from the area where the regions bordered each other. For each area, the background height was subtracted from the protein layer height to get a thickness value. A similar method of calculate surface roughness was used. **Figure 8** shows fluorescence and AFM images obtained from a single circle of both FITC and TRITC-labeled microcontact printed

proteins. **Table 1** shows the resulting overall average thickness and roughness for the FITC and TRITC proteins. The average thickness of the FITC protein layer deposited onto the nanoporous substrate was 8.496 nm with a standard deviation of 1.064 nm. The average surface roughness was 0.301 nm. The average thickness of the deposited TRITC protein layer was 9.271 nm with a standard deviation of 1.075 nm. The average surface roughness was 0.656. The dimensions of IgG have been reported as 8.5 nm × 14.4 nm × 4 nm [21]. The height dimensions observed for the printed protein molecules are consistent with these accepted dimensions for rabbit IgG. This indicates that the microcontact printing method was, on average, able to consistently deposit a single monolayer of rabbit IgG antibodies onto the surface of the nanoporous silica substrate. Furthermore, the average surface roughness is relatively low (at most 0.66 nm), indicating the layer deposited onto the substrate is relatively uniform in coverage [17].

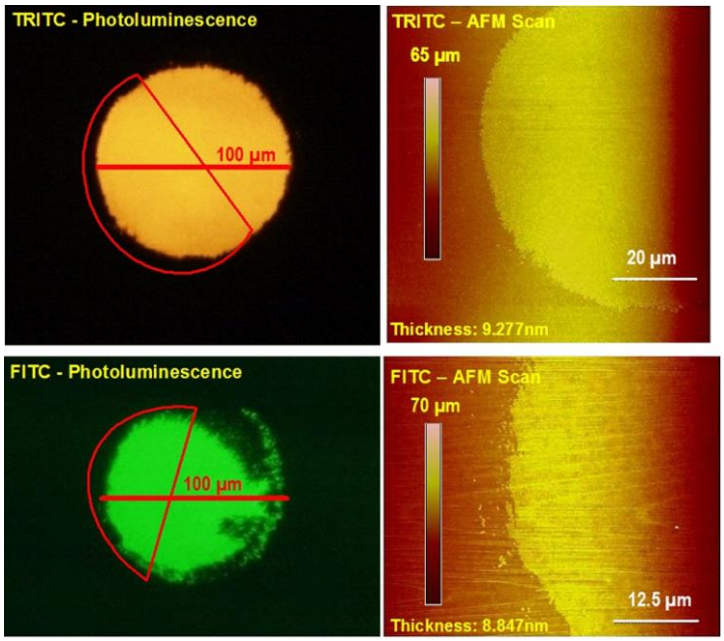

Figure 8. Quantification of Printed Protein Layers. *Fluorescence and AFM images of both FITC and TRITC labeled circular microcontact printed proteins.*

Table 1. *Thickness and roughness measurements of printed proteins.*

Proteins	Number of Samples	Thickness (nm)	Roughness (nm)	Standard Deviation (nm)
TRITC	5	8.496	0.301	1.064
FITC	10	9.271	0.656	1.075

2.3 Patterned Sandwich Enzyme Linked Immunosorbent Assay

Enzyme linked immunosorbent assay (ELISA) is a technique used to detect the presence of specific proteins or antigens in a sample [37]. There are many different types of ELISAs. The direct ELISA is considered the simplest type of ELISA in which the antigen is directly adsorbed to a plastic plate and detected by an enzyme-antibody complex. Upon addition of the enzyme's substrate, the enzyme will produce a signal, usually a color change, indicating the presence of the antigen. The indirect ELISA is similar to the direct ELISA. However, instead of a single detection antibody, an indirect ELISA uses two antibodies. A primary antibody is used to detect and bind to the antigen while a secondary enzyme-antibody complex is used to detect and bind to the primary antibody. Upon addition of the enzyme's substrate, it is the secondary antibody that displays a signal. The sandwich ELISA fixes a capture antibody to the surface to which the antigen of interest binds to. Primary antibody is then used to detect the antigen, and secondary enzyme-antibody is used to detect the primary antibody [38]. Addition of the enzyme's substrate produces a detectable signal. In fluorescence ELISA, when light of a specific wavelength is shone upon the sample, the antigen-antibody complex will fluoresce and the amount or concentration of antigen in the sample can be inferred by the magnitude or the intensity of the fluorescence signal.

Typical ELISA testing requires long procedures involving the use of microliter well plates as well as generous amounts of reagents for each immunoassay performed, and quantified using spectrophotometry comparisons with standards [37, 39–41]. As proof of principle and demonstration of application, a sandwich ELISA for simultaneous detection of two common food allergens, ovomucoid found in egg white and casein found in milk, was performed. The ability to microcontact print and detect multiple antigens in a single sitting, coupled with

fluorescence optical detection and quantification, lays grounds for the potential of creating more efficient immunoassays and biosensors. The ability to also miniaturize and microscale the immunoassay itself enables wider, more cost efficient, varieties of biomedical point of care diagnostics.

2.3.1 Protein Sample Extraction

A white hen egg (Hill Country) was purchased from a local grocery store, cracked, and the egg yolk was separated from the egg white. The egg white was diluted in PBS to form a 25 $\mu g\ mL^{-1}$ solution. Skim milk (Oak Farm) was purchased from a local grocery store. The milk was heated to 40 ^{o}C and reacted with 2% vinegar (acetic acid) in a drop by drop technique to separate the two milk proteins, whey and casein. The whey was discarded and the casein was diluted in PBS to form a 25 $\mu g\ mL^{-1}$ solution. Both egg white and milk solutions were then subjected to heated ultrasonification using an ultrasonic cleaner (Crest 275) to further break down the sample into a uniform solution.

2.3.2 Microcontact Printed Sandwich ELISA

Stamps with one pattern (A) of 100 μm circles were inked with a 5 $\mu g\ mL^{-1}$ mouse anti-chicken ovomucoid (Cosmo Bio) capture antibody solution for 20 min. Stamps with a second pattern (B) of 100 μm circles were inked with a 5 $\mu g\ mL^{-1}$ mouse anti-casein kinase 1, γ1 (Sigma Aldrich) capture antibody solution for 20 min. Both stamps were washed with 0.01 M PBS solution and (diH_2O) and dried under N_2 gas. Alignment of the stamps with the substrate surfaces and printing was done manually using the home-built stamping apparatus facilitated by a microscope positioned above the apparatus. Stamps A and B were brought into contact with nanoporous silica substrates for 1 min.

To prevent non-specific binding, 20 µL of 5% bovine serum albumin (BSA) solution was pipetted onto the surface of the substrates over the protein stamped area in a blocking step. The samples were incubated overnight at 4 ^{o}C and then triple washed at 5 min intervals using 0.01 M PBS solution. 20 µL of the egg white sample solution was pipetted onto the surface of substrate A and 20 µL of the milk sample solution, onto the substrate B. Both samples were incubated for

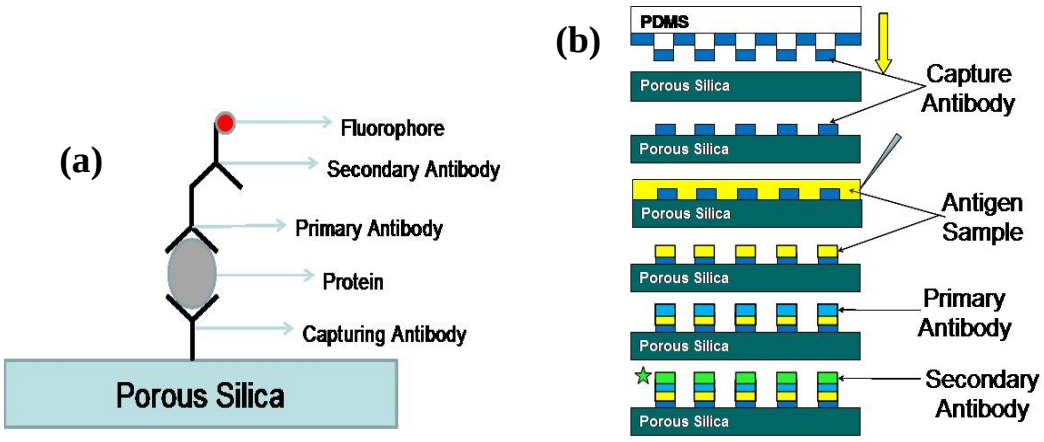

Figure 9. Micropatterned ELISA. *(a) Theoretical molecular structure of a single sandwich ELISA. The ultimate binding of the detecting secondary antibody, tagged by a fluorophore, enables optical detection when excited by a light source. (b) Schematic of the microcontact sandwich ELISA process. The capture antibody is microcontact printed onto the nanoporous silica substrate surface. Subsequent pipetting of specific antibodies builds and completes the sandwich ELISA.*

2 hours at room temperature and then washed in the same manner as previously. 20 µL of 5 µg mL^{-1} rabbit anti-chicken ovomucoid (Alpha Diagnostic International) primary antibody was pipetted onto the surface of substrate A and 20 µL of 5 µg mL^{-1} rabbit anti-casein kinase 1, α1 (Sigma Aldrich) primary antibody, onto substrate B. Samples were incubated for 2 hours at room temperature and then subjected to a washing step. 20 µL of 5 µg mL^{-1} of FITC-tagged anti-rabbit IgG was pipetted onto the surface of substrate A and 20 µL of 5 µg mL^{-1} of TRITC-tagged anti-rabbit IgG, onto substrate B. Samples were incubated for 1 hour at room temperature and then subjected to a final washing step. **Figure 9** shows the schematic for microcontact printed sandwich ELISA process and the theoretical molecular structure of a single microcontact printed

sandwich ELISA on the surface of a nanoporous silica substrate. Each substrate was viewed by fluorescence microscopy (Olympus BX51) for positive detection of component antigens.

2.3.3 Results and Discussion

The ability to incorporate the μCP technique to perform a sandwich ELISA on the surface of a nanoporous silica substrate was demonstrated. The detection of common allergens egg white protein ovomucoid and milk protein casein was performed. The two sample substrates were observed under a fluorescence microscope under FITC and TRITC filters. Both samples fluoresced under their respective filters indicating positive detection of the allergens and successful microcontact printed sandwich ELISAs. FITC-detected ovomucoid fluoresced green under the FITC filter while showing little to no fluorescence under the TRITC filter. TRITC-detected casein fluoresced red-orange under the TRITC filter while showing little to no fluorescence under the FITC filter. The detection method was therefore successfully specific to the desired allergen under examination. **Figure 10** shows the fluorescence microscopy pictures of both sample substrates.

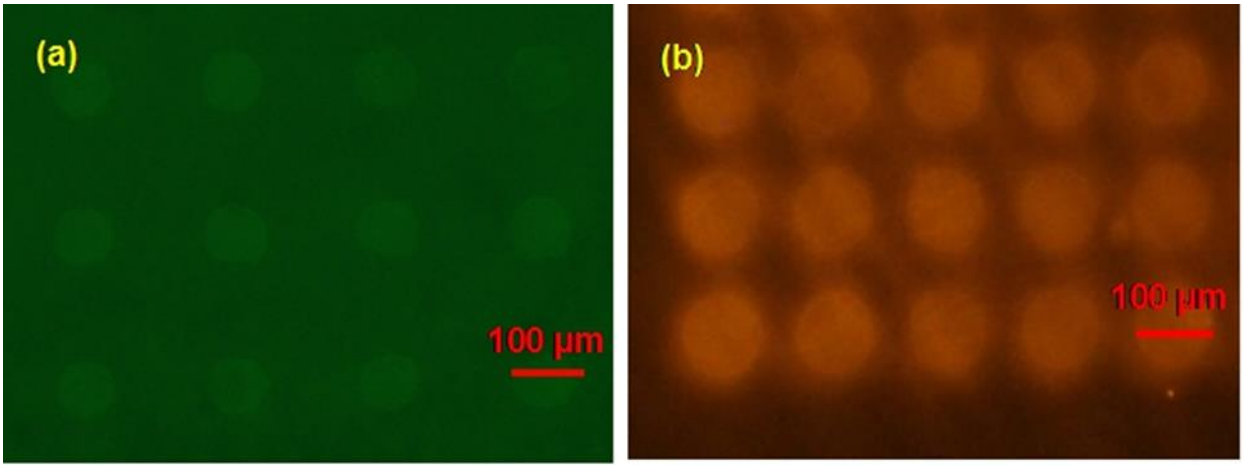

Figure 10. Fluorescence Imaging of Micropatterned Sandwich ELISA. *Fluorescence microscopy pictures of the microcontact printed sandwich ELISAs on nanoporous silica substrates. (a) FITC-tagged egg white ovomucoid and (b) TRITC-tagged milk casein.*

2.4 Conclusion

In this part of the thesis, a method for multicolor microcontact printing on nanoporous silica substrate that allows from more efficient detection of multiple proteins on a single substrate with a potential for enhancing diagnostic power of immunoassays was described. In addition, it was demonstrated that the method had the capability to perform a miniaturized sandwich ELISA to detect common food allergens, such as egg white ovomucoid and milk casein, on nanoporous silica substrate using the microcontact printing technique. The use of nanoporous silica membranes as substrate material allows versatile surface functionalization and provides for better protein adhesion and adsorption. The ability to microcontact print multiple proteins onto the same substrate surface allows for high-throughput manufacturing of compact systems with planar device structures, ideal for detection on-chip designs. Furthermore, such capability has great potential in increasing the efficiency of immunoassays, such as sandwich ELISAs, with the ability to detect two antigens simultaneously. With further extension of the multicolor microcontact printing method described here, a sandwich ELISA of two different

antigens could be conducted on the same substrate. Food samples containing both egg white and milk would be able to be detected simultaneously on the same substrate.

Most importantly, μCP on nanoporous silica can have large impact on the effectiveness and efficiency of capturing cancer cells for cancer cell detection in applications of cancer diagnostics and detection. Such an application will be demonstrated in later sections.

3 Quantum Dots as Contrast Agents

Conventional fluorescence labeling and markers have typically been organic dyes, such as fluorescein isothiocyanate (FITC) and tetramethyl rhodamine isothiocyanate (TRITC), and many researchers have long been seeking answers to their many limitations. Organic dyes are not photostable and photobleach under light exposure or long term storage. They also exhibit only single excitation and single emission wavelengths. In recent years, quantum dots (QDs) have been growing and receiving much attention in addressing the limitations presented by organic dyes.

QDs are nanoparticles, or more specifically nanocrystals, with tunable emission wavelengths and are composed of semiconductor material, usually cadmium or zinc. Because QDs are semiconductors, they have electrical conductivity between that of a conductor and an insulator. Metals are highly conductive due to a large density of available states in which electrons can occupy in the Fermi level, the highest occupied molecular orbital in the valance band or the energy below which there is a 50% chance of finding an occupied energy state. Electrons can therefore move freely between energy levels. Insulators on the other hand, have large energy band gaps between the electron-occupied energy levels and empty energy levels, limiting electron motion. Semiconductors therefore have an intermediate level of electric conductivity. They have a band gap small enough for sufficient numbers of electrons to jump from the lower energy valance band to the conduction band. This movement of electrons creates electron holes in the valance band and the presence of loosely held electrons in the conduction band. Furthermore, electrons may move around to fill a hole contributing to electrical conductivity [42].

The size of the QDs determines the wavelength it emits allowing for tunable emission wavelengths (shown in **Figure 11**), making them attractive for multicolor detection systems. This unique characteristic of QDs can be attributed to quantum confinement. In the semiconductor crystal lattice, electrons are squeezed together, a phenomena explained by the Pauli exclusion principle, which states that no two electrons can simultaneously occupy the same quantum state. The number of energy levels are therefore determined and restricted by the size of the QD. Smaller QDs have a larger band gap and therefore a greater difference in energy between the highest valence band and the lowest conduction band. More energy is needed to excite the QD which in turn, results in larger amounts of energy released when the QD returns to resting state. In contrast, larger QDs have a smaller band gap and less energy is needed to excite the QD, resulting in less energy released when the QD returns to resting state. Because of this size-tunable advantage, high levels of synthesis control over fabrication can be used to implement precise control over the conductive properties of the material [42–45].

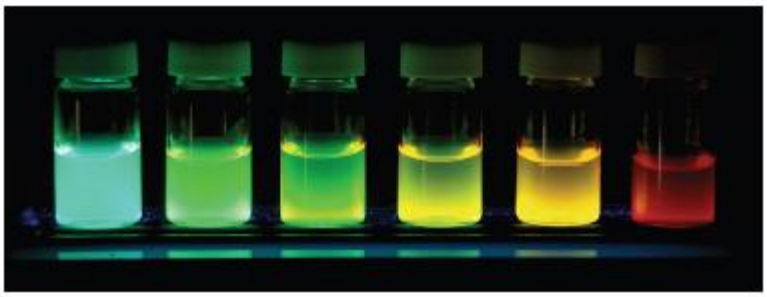

Figure 11. Synthesized Colloidal QDs. *QDs made of CdSe:ZnS. QDs exhibit broad excitation range and narrow single wavelength emission allowing them to be excited with a single light source. This unique multicolor property of QDs is due to their size-tunable advantage [46].*

Another key advantage QDs have, is their capability to be excited by a single excitation light source. They have a broad absorption range and single emission wavelength, allowing for simultaneous excitation and viewing of multiple fluorescence markers with a single excitation

light source. This advantage is attributed to the quantum confinement and size-dependent characteristic of QDs. High energy excitation light sources with shorter wavelengths, such as UV light sources, can easily excite QDs of any size resulting in an emission of lower energy and longer wavelengths in the visible light range of the electromagnetic spectrum. Due to quantum confinement, the energy and wavelength emitted is defined by the size of the QD and can be described as the sum of the band gap energy between occupied levels and unoccupied energy levels. This advantage provides the ability for multicolor immunofluorescence assays capable of distinguishing between different cancer cell lines. Additionally, QDs are brighter due to higher quantum yield and are more photostable than organic dyes thus enabling them to be exposed to light during long term storage without photobleaching. This advantage makes the microchip-based cancer cell detection system capable of post screening analysis and imaging [42, 46, 47].

The recognition of the many advantages of QDs has led to an explosion of biological applications of QDs. One of the most rapidly growing applications is the use of QDs as imaging agents in in vitro imaging and detection of various cancer cell types (shown in **Figure 12**), such as prostate, breast, and pancreatic cancer [46, 48–51]. Detection and imaging for living cells in culture involve a simple detection via cancer cell biomarker specific labeled antibodies that are conjugated with QDs. However, unlike the monolayers of cultured cells and thin tissue sections, challenges arise with increase in complexity to multicellular

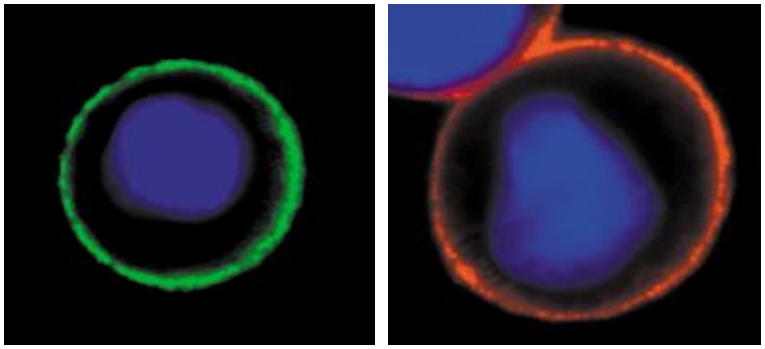

Figure 12. Detection of HER2 with QD-IgG. *Breast cancer SkBr3 cells were incubated with monoclonal anti-HER2 antibody and fluorescently labeled with QD-labeled goat anti-mouse IgG. The cell on the left was labeled with QD535 IgG while the cell on the right was labeled with QD630 IgG [49].*

organisms where tissue thickness becomes a major concern. Biological tissue attenuates imaging signals. QDs have allowed for the fluorescence imaging of various biological tissues, such as blood vessels and lymph nodes [51].

Another application QDs have been prominently used in is fluorescence resonance energy transfer (FRET) which involves the transfer of fluorescence energy from donor particle to an acceptor particle when the distance between the two is smaller than a critical radius, or the Foerster redius. QDs in FRET technologies can be used in immunoassays when they are conjugated to biological molecules, such as antibodies. QDs act as donors in assays. An example of bioconjugated QDs as biosensors is in quantitative maltose sensing where QDs are conjugated to maltose binding protein (MBP) and bind to either maltose or a quenching molecule which has a binding affinity similar to that of maltose. Upon addition of maltose, the quenching molecule is displaced and a concentration dependent increase in luminescence is observed. As demonstrated by this particular application, QDs make for a very reliable, stable, and bright detection and imaging system.

The unique advantage of QDs' characteristic broad excitation range and narrow single emission has garnered much attention in developing multicolor imaging systems. One such imaging system is hyperspectral microscopic imaging (HMI). HMI utilizes the various wavelengths across the electromagnetic spectrum to provide detailed images with more information than those provided by conventional microscopic imaging. Therefore, HMI with multiple fluorophore labeling is an effective tool for distinguishing between various cancer cell types. HMI has been employed to simultaneously image ten different tumor markers of a cell, as shown in **Figure 13**. Ultimately, by integrating QD-labeled cancer cells with the HMI process,

brighter and stabler photoluminescence can be achieved while simultaneously identifying various biomarkers in cells, enhancing specificity of detection and identification [52].

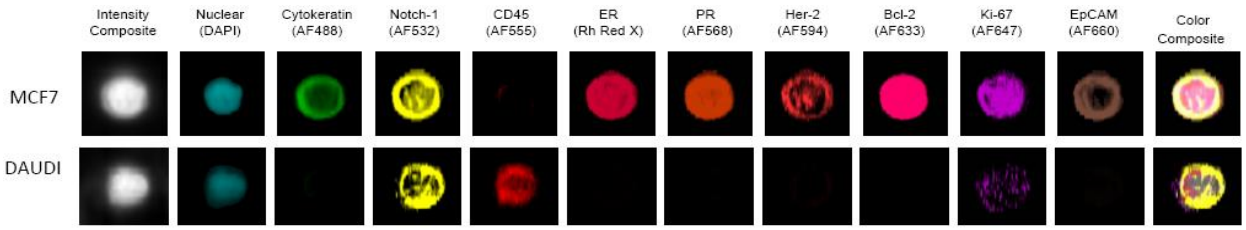

Figure 13. HMI Cancer Cell Imaging. *Quantification of ten fluorescent markers by HMI [38].*

QDs have also been used in combination with various other nanotechnologies to create light source platforms that can potentially form the foundation for illumination of biological samples. QDs have been used in conjunction with the μCP technique in electronics and optoelectronics such as light-emitting diodes (LEDs) and solar cells [33, 53, 54]. Gopal et al. has previously demonstrated localized electroluminescence for multicolor illumination of cancer cells on a single chip (see **Figure 14**) [55]. Stained cancer cell samples on a cover slip were placed over a multicolor QD-LED source and observed under a microscope while imaging the cells at different excitation wavelengths. Because different parts of cells fluoresce when excited by specific wavelengths, the platform was capable of imaging various parts of the cells under different excitation wavelengths. This application of QDs shows the utilization of QDs and its advantages to create an effective biological microchip-based imaging platform. In addition, it demonstrates the strength of combining various nanotechnologies into a single microchip platform that utilizes the advantages of each nanotechnology for effective biological applications. Similarly, the platform described in this thesis emphasizes the combination of various nanotechnologies and their advantages in a microchip based platform for biological applications, specifically, in cancer cell detection.

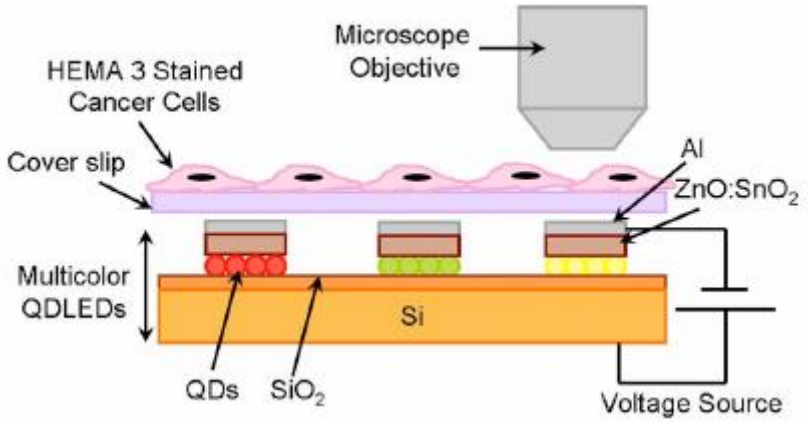

Figure 14. Integrated Bioimaging System. *Schematic of the integrated QD-LED microchip-based platform for the QD fluorescence imaging of cancer cells [55].*

In the work presented in this thesis, QDs are primarily used for the photostable and bright imaging of captured cancer cells on a micropatterned nanoporous silica substrate. QD imaging is an added advantage to the microchip-based platform, potentially extending the lifetime and shelf life of the chip post-screening and providing medical analyzers with an easy-to-spot and bright fluorescence signal for the detection of rare CTC cells in blood samples.

4 Fundamentals of Microfluidic Channels

Recent years have shown growing interest in microfluidic channels as biomedical devices in the clinical and point-of-care settings due to the advantages the channels incur on a microscale level. Microfluidics decrease the volume of reagents and samples needed to run an experiment, usually down to the micro or even nanoliter scale, making it extremely cost-effective. Microfluidic channels are also easy to design, fabricate, and mass produce using microfabrication and lithographic techniques. Multiple channels can be further used to achieve high throughput capabilities, reducing the amount of time needed to perform experiments and data analyses. The advantages of integrated microfluidic microchips allow for various functions to be performed on a micro or nanoscale level, especially for biologics and medical applications. Microchannels geometrically confine fluids to a sub-millimeter scale allowing for precise control and manipulation of fluids. Microfluidics have been used for DNA amplification and analysis [56–58], flow cytometry [59–61], immunoassays [15, 42–44], and point-of-care diagnostics [65].

Behavior of fluids at the microscale level can differ greatly from that at the macroscale level. Factors such as surface tension, energy dissipation, and fluidic resistance begin to dominate the system. Fluid flow relative to the static walls within a straight microfluidic channel can be characterized by the Reynolds number (Re) given by:

$$Re = \frac{\rho v L}{\mu} \qquad \text{— (1)}$$

where ρ = density of the fluid, v = mean velocity of the object relative to the fluid, L = characteristic linear dimension, μ = dynamic viscosity of the fluid. The Re is a ratio between the inertial forces to viscous forces on the fluid. Flow in a microfluidic channel can be described as

laminar flow, where the Re is less than 2300, and the streamlines are steady and parallel to the direction of fluid movement (shown in **Figure 16**) [66, 67].

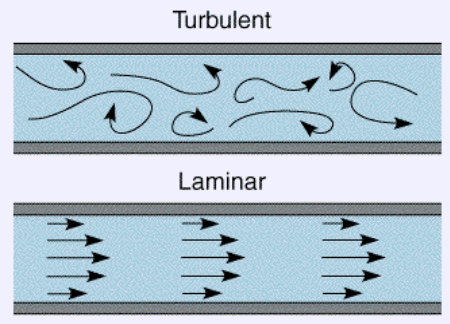

Figure 16. Flow Profiles within a Tube. *Turbulent flow, shown in the top figure, exhibits a fluid with chaotic flow and no distinct streamlines. In contrast, laminar flow, shown in the bottom figure, exhibits a fluid with distinct streamlines that are parallel to the direction of fluid movement. Microfluidic channels are characterized by laminar flow [66].*

Microfluidic channels of various geometries can be fabricated and realized through simple microfabrication techniques. In addition, the ability to mass produce microchannels in a relatively straightforward and simple method reduces the cost of fabrication. Most of the microfluidic channels used in biological applications are made from polydimethylsiloxane (PDMS) molding which is a negative imprint of a silicon master. With current photolithographic technologies, creating the silicon master on a silicon wafer is relatively easy and time efficient. Briefly, patterns are designed on a computer-aided design (CAD) program and printed onto a mask. A silicon wafer is spin coated with photoresist, usually SU-8, to the thickness of the desired channel height. The mask is placed on top of the photoresist and exposed to UV light. The photoresist is then further developed in developing chemical to reveal a patterned silicon wafer. Once the master is created, simple polymerization of PDMS in the mold will yield the desired microchannel (see

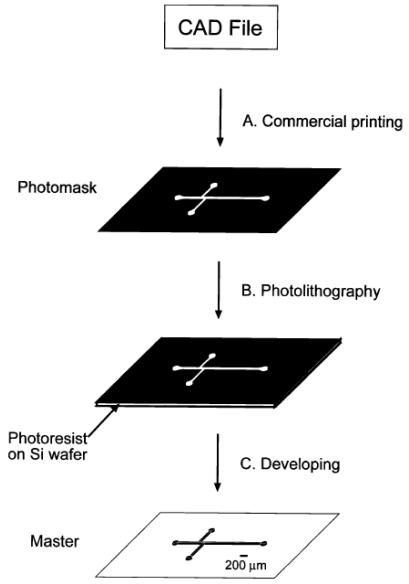

Figure 15. Silicon Lithographic Fabrication of Microfluidic Channels. *Schematic of the fabrication of silicon masters for microfluidic channels via soft lithographic methods. After the master is fabricated, PDMS polymer can be poured into the master to create the microchannel [68].*

Figure 15) [68]. Such easy fabrication methods has allowed microfluidic channels to be designed and fabricated rapidly and inexpensively, making them attractive for use in various biological applications and components for integrated systems.

The advantages that microchannels embody have been utilized in many biological applications. One of the more predominate applications is the capturing and detection of CTCs. One example of a microfluidic-based CTC screening system has been demonstrated by Hoshino et al. (see **Figure 17**) [69]. The microchip CTC screening system utilizes the advantages of the localized confinement defined by a microfluidic channel to perform immunomagnetic detection of CTCs. Microfluidics aided in the design and development of a low cost, highly specific and sensitive miniaturized screening platform by reducing reagent and sample volume and exposing nanoparticle-labeled cancer cells to a more localized magnetic field.

Integration of microfluidic channels with microcontact printed nanoporous silica based microchips can enhance the capture of cancer cells. The microchannel can be designed to increase the binding interactions between microcontact printed antibodies on the nanoporous silica substrate and cellular biomarker antigens present on the cell surface. Furthermore, the laminar flow that characterizes microfluidic channels can be disrupted, and turbulent flow can be introduced

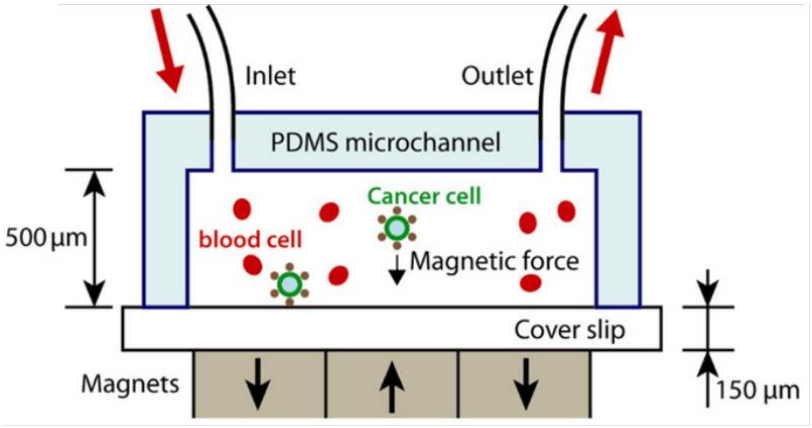

Figure 17. Microchip-based Immunomagnetic Detection of Cancer Cells. *Schematic of the immunomagnetic detection of cancer cells. The microfluidic channel aids in bringing nanoparticle-labeled cancer cells closer to the magnets below the cover slip. In addition, the confinement of reagents and samples to a small volume reduces cost effectively [69].*

through the utilization of grooved microchannels. Grooved microchannels create a micromixed environment within the channel and therefore brings cells even closer to the surface, increasing the probability for cell-surface interactions [70–72].

Grooved microchannels have been examined as a method to introduce turbulent flow into the otherwise laminar environment that characterizes the flow within a straight microchannel. One of the more prominently looked at methods and designs for such channels are the micropillars and herringbone structures first introduced by Nagrath et al. and Stott et al., in the CTC-Chip [70] and the HB-Chip [73], respectively (see **Figure 18**). In both cases, the micropillars and the herringbone structures introduced a micromixing environment within the channel that brought the cells closer to the surface of the microchip, allowing for enhanced interactions between the capture antibodies coated on the micropillars or within the microchannel and the biomarkers on the surface of the cancer cell. In addition, optimal surface interaction geometry was characterized for the herringbone structure microchannels. It was found that groove widths of about 125 µm were optimal for cell-surface interactions.

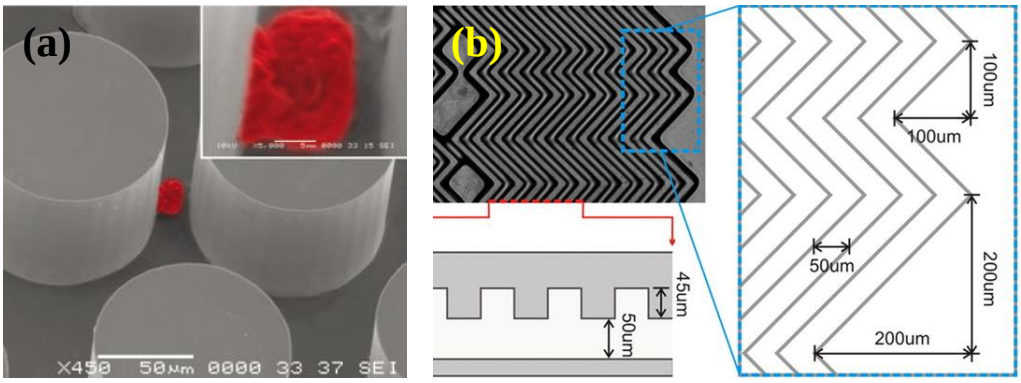

Figure 18. CTC-Chip and HB-Chip. *The CTC-Chip and HB-Chip introduces physical obstacles within the microfluidic channel in order to create a micromixing environment within the channel. The CTC-Chip (a) uses EpCAM-functionalized micropillars and the HB-Chip (b) uses EpCAM coated microchannel with herringbone structures [73].*

Aside from cancer cell detection, microfluidic channels have been used in other applications, such as biosensors, drug delivery systems, and biomimetic systems [74–76]. Biomimetic systems in microfluidic channels have helped provide a miniaturized system on a microchip platform for various biological studies. Huh et al. developed the lung-on-a-chip, a flexible biomimetic chip designed to mimic the mechanical and biochemical behaviors of the human lung [74]. Through use of microfluidics, Huh was able to reconstitute the functional alveolar-capillary interface of the lung (see **Figure 19**). The culturing of cells into tissue or even whole organ systems provides a large advantage to understanding the basic fundamental biology of certain diseases. Such systems provide useful and effective platforms for drug studies and the cellular interactions that result in detrimental human diseases. Wu et al. developed a microfluidic platform designed to culture self-assembled tumor spheroids [76]. The platform allows for

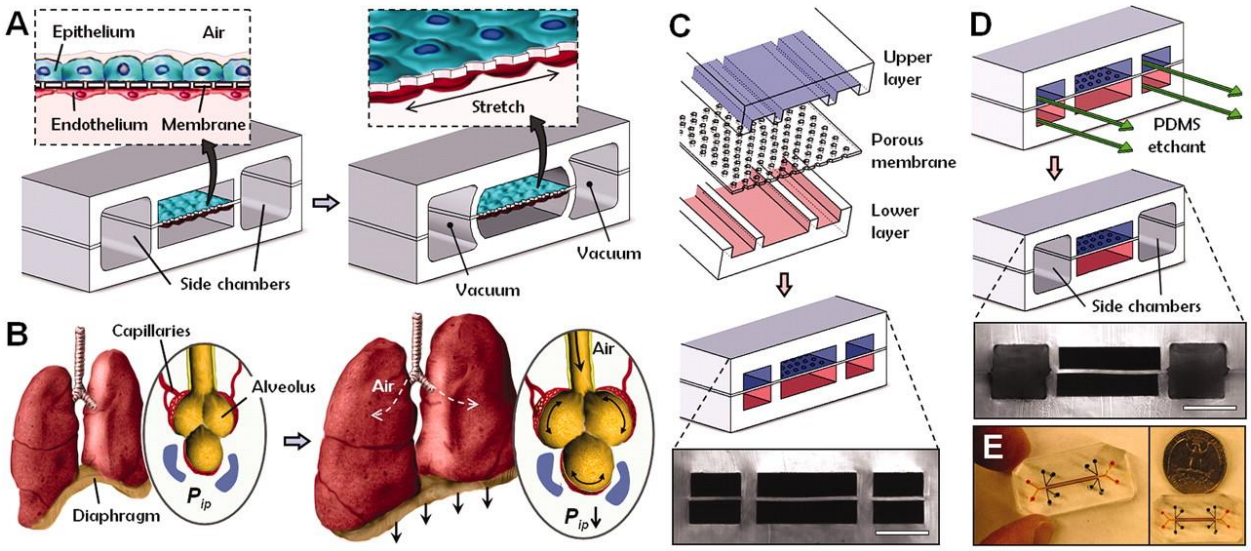

Figure 19. Lung-on-Chip. *(A) The biomimetic microchip uses compartmentalized PDMS microchannels to form an alveolar-capillary barrier on a flexible PDMS membrane coated with ECM. (B) During inhalation in the lung, contraction of the diaphragm causes a pressure change that stretches the alveolar-capillary interface. (C) Three PDMS layers are aligned and bonded to form two sets of three parallel microchannels separated by a porous PDMS membrane. (D) PDMS etching is flowed through the side channels that leads to selective etching of the membrane layers to produce two large side chambers to which vacuum is applied to cause mechanical stretching. (E) Top view images of the actual lung-on-a-chip microfluidic device [74].*

further studies on the interactions of cancer cells on a cellular level and observation of the formation of tumors. In addition, it provides a platform for anticancer drug discovery.

In this thesis, microfluidic channels are used in enhancing cancer cell detection. A design example is presented in this thesis, consisting of a microchannel 20 mm long and 200 μm high, constructed with two grooves, each 5 mm wide, 100 μm deep, and spaced 3 mm apart from each other. The grooved microchannel presented in this thesis illustrates the ability to modify the channel geometries to enhance cell capture and cell-surface interactions by introducing micromixed environments within the channel. Additionally, site-specific capturing of cancer cells can be performed in accordance to channel geometries via simulations and modeling to determine optimal locations for cell capture within the microchannel.

5 Patterned ELISA Cancer Cell Detection

This section of the thesis describes an application of three of the four technologies described and introduced in the first half of the thesis to perform immunofluorescence detection of QD labeled cancer cells. Here, the μCP technique is employed in the patterning of capture antibodies on nanoporous silica substrates, specifically anti-epithelial cell adhesion molecule (anti-EpCAM), in the capturing of breast cancer cells from cell line SkBr3 and colon cancer cells from cell line Colo205. As previously mentioned, SkBr3 and Colo205 cells have been known to overexpress EpCAM biomarkers on the cells' surface [8]. In addition, SkBr3 cells have been known to overexpress anti-human epidermal growth factor receptor 2 (anti-HER2), while Colo205 cells display cytokeratin (CK) proteins. The method of detection is similar to that of a direct enzyme-linked immunoabsorbent assay (ELISA), where the capture antibody is microcontact printed on the substrate surface and subsequently used to capture SkBr3 and Colo205 cells onto the substrate, followed by fluorescence detection. Here, fluorescence detection and imaging of SkBr3 and Colo205 cells was performed using quantum dot (QD) labeled anti-HER2 and FITC labeled anti-CK detecting antibodies, respectively.

5.1 Experimental Methods

5.1.1 Cell Culture

SkBr3 and MDA-MB-435 breast cancer cells were cultured in RPMI 1640 media, supplemented with 20% fetal bovine serum (FBS) (Gibco®, Invitrogen), and incubated in a humidified incubator (37 ^{o}C, 5% CO_2). The cells were passaged biweekly or when needed, as follows. Old media was aspirated from the culturing plate and 5 mL phosphate buffer saline (PBS) was pipetted into the plate to rinse the cell layer. The PBS was aspirated and 3 mL of

trypsin (Gibco®, Invitrogen) was pipetted into the plate and incubated for 10 min. After incubation for 10 min, 3 mL of media was pipetted into the plate to neutralize the trypsin and stop trypsinization. The cell suspension was pipetted into a conical centrifuge tube and centrifuged at 1000 rpm for 3 min. The supernatant was aspirated, leaving behind the cell pellet which was then resuspended in 1 mL media. A fraction of the cells were then pipetted into a new cell culture petri dish with 10 mL fresh media. Colo205 colon cancer cells were cultured in the same manner without trypsinization. Colo205 cells were centrifuged, resuspended in media, and split into a petri dish of fresh media. When needed for experimentation, cells were resuspended in PBS. Cell counts were performed using a hemocytometer (Hausser Scientific). A volume containing the desired number of cells was extracted from the cell suspension and resuspended in 3 mL PBS in a new centrifuge tube.

5.1.2 Microcontact Printing of Capture Antibody

Polydimethylsiloxane (PDMS) stamps were fabricated using a mixture of 10:1 Sylgard 184 silicone elastomer to curing agent (Dow Corning). The mixture was vigorously mixed and then placed in a desiccator to remove extraneous bubbles. The resulting mixture was carefully poured into a petri dish and extra bubbles were removed by blowing. The PDMS mixture was allowed to cure overnight at room temperature. When needed, the cured polymer was peeled from the silicon mold and cut into stamps with 5 mm x 5 mm square area.

Stamps were inked with the capture antibody, a 30 µg/mL anti-EpCAM solution, for 20 min then washed with PBS and diH_2O, and dried under N_2 gas. **Figure 20** shows the basic schematic for µCP proteins onto a nanoporous silica substrate. The stamps were brought into contact with the nanoproous silica substrate for 1 min. Printing was done manually using a home built mechanical apparatus. The apparatus consists of a stamp-carrying magnetic piece capable of micrometer translations in the x, y, and z directions allowing alignment precision within 5 µm. To visualize the alignment of the stamp with the substrate and the actual contact between stamp and substrate, a microscope was positioned above the apparatus.

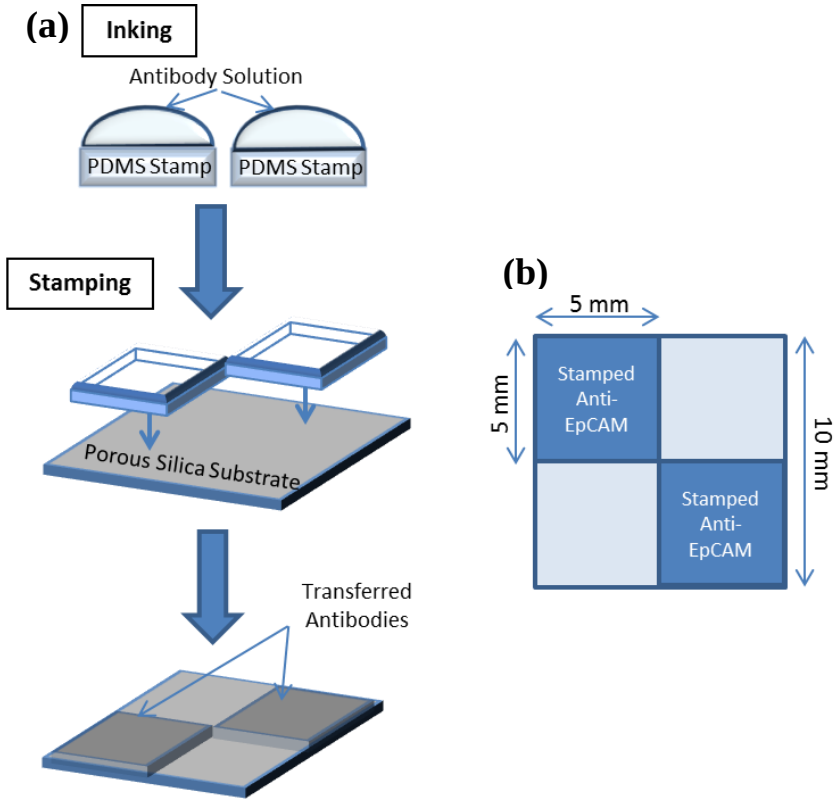

Figure 20. Microcontact printing process. *(a) PDMS stamps are first inked with desired antibody solution and then stamped onto the porous silica substrate through direct physical contact. (b) A design of 10 mm x 10 mm nanoporous silica substrate with anti-EpCAM patterned 5 mm x 5 mm square areas.*

Transferred antibody layers were characterized using atomic force microscopy (AFM; Digital Instruments Series IV, Veeco) for surface thickness and roughness to show uniform monolayer deposition of proteins.

5.1.3 Immunofluorescence Detection of QD Labeled Cancer Cells

Here, QDs with an emission wavelength of 625 nm (QD625) were purchased as a part of a conjugation kit (Invitrogen). They were conjugated with anti-human epidermal growth factor receptor 2 (HER2) antibodies (Sigma Aldrich) via the conjugation method provided along with the kit. 10 µL of the QD625-labeled anti-HER2 (50 µg/mL) was pipetted into the previously prepared SkBr3 cell suspension (20,000 cells). The cell suspension was then placed into an incubation oven for 2 hour at 37 ^{o}C. Fluorescein isothiocyanate (FITC) labeled anti-cytokeratin (CK, 20 µg/mL) (Sigma Aldrich) was pipetted into the previously prepared Colo205 cell suspension (20,000 cells). The cell suspension was then placed into an incubation oven for 1 hour at 37 ^{o}C. MDA-MB-435 cells were left unlabeled.

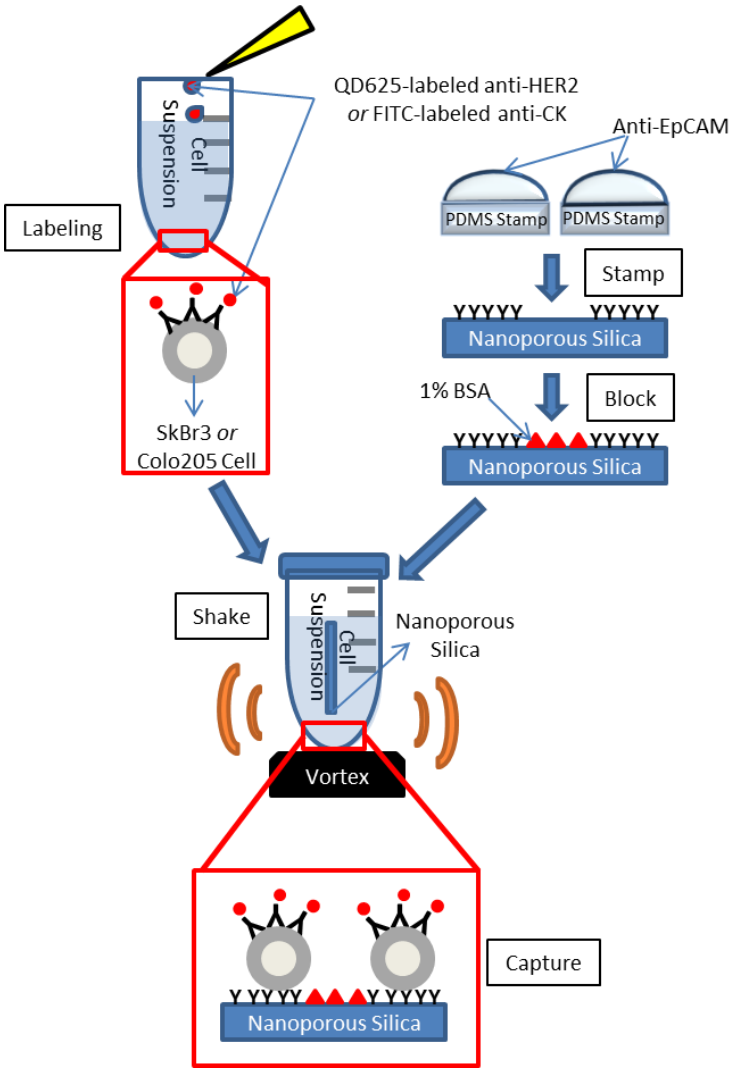

Figure 21. Immunofluorescence Detection of QD-Labeled Cancer Cells. *Microcontact printing process of antibodies (anti-EpCAM) on nanoporous silica substrate for immunofluorescence detection of labeled (QD625 or FITC) cancer cells (SkBr3 or Colo205).*

To prevent non-specific binding, the surfaces of the anti-EpCAM stamped nanoporous silica substrates were blocked using a 1% bovine serum albumin (BSA)

solution at 37 ^{o}C for 30 min. After blocking, the substrates were triple rinsed with PBS for 5 min intervals. The substrates were then placed into the three separate prepared cell suspensions (QD625-labeled SkBr3, FITC-labeled Colo205, and non-labeled MDA-MB-435) and placed on a vortex machine in a styrofoam conical centrifuge tube holder. The conical tubes were allowed to shake on the vortex machine at the lowest setting (Shake 1) for 3 hour at room temperature. The shaking motion that the vortex machine provides creates a slightly dynamic environment for the cells to have higher probability of interaction with the nanoporous silica substrate, and also serves to prevent cells from sinking to the bottom of the tube where they could remain sedentary. After 3 hour, the substrates were removed from the conical tube and gently placed into PBS for 5 min to rinse off remaining free loose cells. Extraneous liquid was removed using Kimwipes. The substrates were placed into the freezer and allowed to freeze for 10 min at 4 ^{o}C. Captured cells on the nanoporous silica substrate were fixed with glacial acetone in the freezer at 4 ^{o}C for 10 min. The nuclei of the cells were stained with DAPI. Each substrate was viewed by fluorescence microscopy (Olympus IX2-UCB). The number of cells in each test area was counted in a top to bottom fashion while incrementally moving in the translational direction. **Figure 21** shows a schematic of the whole process of μCP of antibodies on nanoporous silica thin film substrate for immunofluorescence detection of labeled cancer cells.

5.1.4 Statistical Analysis

Statistical analysis was performed for the comparison of cell capture numbers between different conditions for a total of five experiments each performed under the same conditions (**Section 5.1.3**). The averages and standard deviations were tabulated for each experiment's data set and the ANOVA test was used to make comparisons. Assumptions used when performing the

ANOVA test includes normality and equal variance. The ANOVA test uses the *F* statistic which can be calculated using the following equation:

$$F = \frac{MS_{Between\ Groups}}{MS_{Within\ Groups}} \qquad \text{— (2)}$$

where $MS_{Between\ Groups}$= the mean squares between groups and $MS_{Within\ Groups}$= the mean squares within groups.$MS_{Between\ Groups}$ can be calculated using the following equation:

$$MS_{Between\ Groups} = \frac{\sum(\bar{X}_i - \bar{X})^2}{I - 1} \qquad \text{— (3)}$$

where $\bar{X}$= mean for all the data, $\bar{X}_i$= mean of group *i*, and *I* = number of groups. $MS_{Within\ Groups}$ can be calculated using the following equation:

$$MS_{Within\ Groups} = \frac{\sum\left(x_{ij} - \bar{X}_i\right)^2}{n - I} \qquad \text{— (4)}$$

where x_{ij}= value of measurement *j* in group *i*, $\bar{X}_i$= mean of group *i*, *n* = total number of measurements, and *I* = number of groups. The value of the *F* statistic can then be compared to the F(*I* – 1, *n* – *I*) distribution and a *p*-value is obtained. A *p*-value of less than 0.05 indicates that the means within the groups are statistically different and the null hypothesis is rejected. A *p*-value greater than 0.05, indicates that the means within the groups are not statistically different and the null hypothesis is accepted. However, only performing the ANOVA test did not indicate which pairs were different; therefore a method that accounts for multiple data sets, such as the Tukey's Method (a post hoc test), was used.

For the different experimental conditions, the data obtained were compared using the ANOVA test for differences. All ANOVA tests were performed using the MATLAB function anova1. A comparison between multiple data sets was then performed using the MATLAB multcompare function to determine which pairs were different.

5.2 Results and Discussion

5.2.1 Characterization of Printed Capture Antibody

The stamped anti-EpCAM layers were analyzed using AFM microscopy and NanoScope Analysis to determine the consistency of the transfer of the antibody from PDMS stamp to the nanoporous silica substrate. Five stamped areas were arbitrarily chosen on the substrate and evaluated for antibody layer thickness and surface roughness. Thickness data were calculated by dividing AFM images into regions of antibody coverage and regions of nanoporous silica substrate background. The background height was then subtracted from the protein layer height to obtain a thickness value. A similar method of calculating surface roughness was used within a 1 µm x 1 µm square area. **Figure 22** shows an AFM image obtained from an area of microcontact printed anti-EpCAM along with the cross section plot of the sample. The average thickness of the antibody layer deposited onto the nanoporous silica substrate was 6.07 ± 1.70 nm. The thickness dimensions are relatively consistent with the antibody dimensions previously reported [21]. This indicates that the microcontact printing method was able to deposit a monolayer of anti-EpCAM antibodies onto the surface of the nanoporous silica substrate. The average surface roughness was 0.54 ±

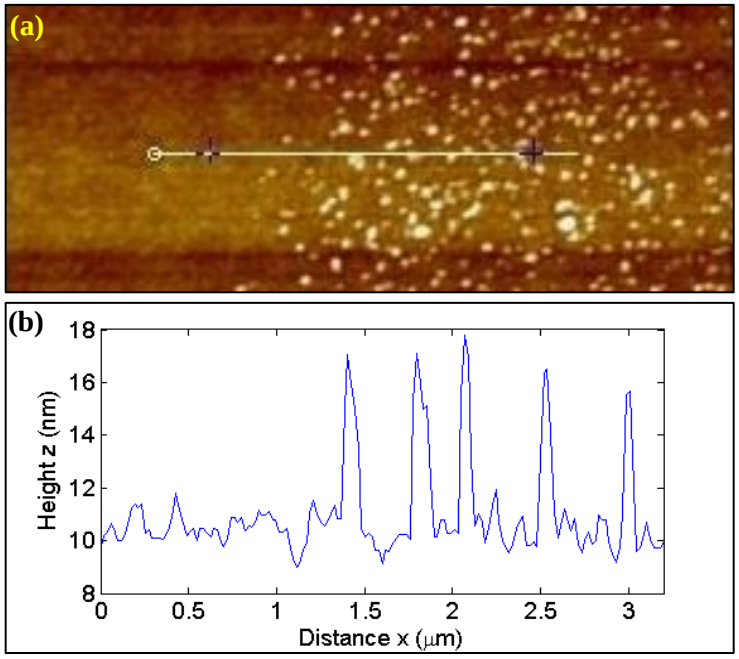

Figure 22. Characterization of Patterned Nanoporous Substrates. *AFM characterizations of microcontact printed anti-EpCAM on nanoporous silica substrate: (a) thickness and roughness of antibody layer and (b) the cross section plot of the sample.*

0.32 nm. This low average surface roughness indicates that the antibody layer deposited is relatively uniform in coverage.

5.2.2 Immunofluorescence Detection of QD Labeled Cancer Cells

SkBr3 breast cancer cells were labeled with QD625-labeled anti-HER2, while Colo205 colon cancer cells were labeled with FITC-labeled anti-CK. The SkBr3 and Colo205 cells were captured via antibody-antigen interactions between the cell surface and the stamped nanoporous silica substrate surface. Non-labeled MDA-MB-435 cells were used as a negative control. Non-stamped areas of the substrate also served as a negative control. Fluorescence images were observed to verify and distinguish the presence of the various cells. SkBr3 cells are EpCAM positive and HER2 positive cells, and should therefore be captured on the substrate, labeled with QD625-labeled anti-HER2, and positive in DAPI. Colo205 cells are EpCAM positive and CK positive cells, and should therefore be captured on the substrate, labeled with FITC-labeled anti-CK, and positive in DAPI.

Figure 23a shows the identification of captured SkBr3 cells under the DAPI filter, under a filter cube (excitation peak wavelength 577 nm, bandwidth 20 nm; dichroic mirror 595 nm long-pass; emission peak wavelength 630 nm, bandwidth 30 nm) and as an overlay of the two previous images under 20X magnification. **Figure 23b** also shows the identification of a captured Colo205 cell under the DAPI filter, under the FITC filter, and as an overlay of the two previous images under 20X magnification. DAPI images were taken at an exposure time of 5 ms, QD625 images at an exposure time of 3 s, and FITC images at an exposure time of 150 ms. The nucleus of the cells, stained with DAPI fluoresced blue while the HER2 receptors on the surface of SkBr3 cells fluoresced red and the CK proteins of the Colo205 cytoskeleton fluoresced green. **Figure 23c** also contrasts the captured cell density within a defined area of no stamped anti-

EpCAM antibodies with the captured cell density within an area with stamped anti-EpCAM on the nanoporous silica substrate. It can be seen that the captured cell density within the area of no stamped anti-EpCAM is lower than that within the area with stamped anti-EpCAM.

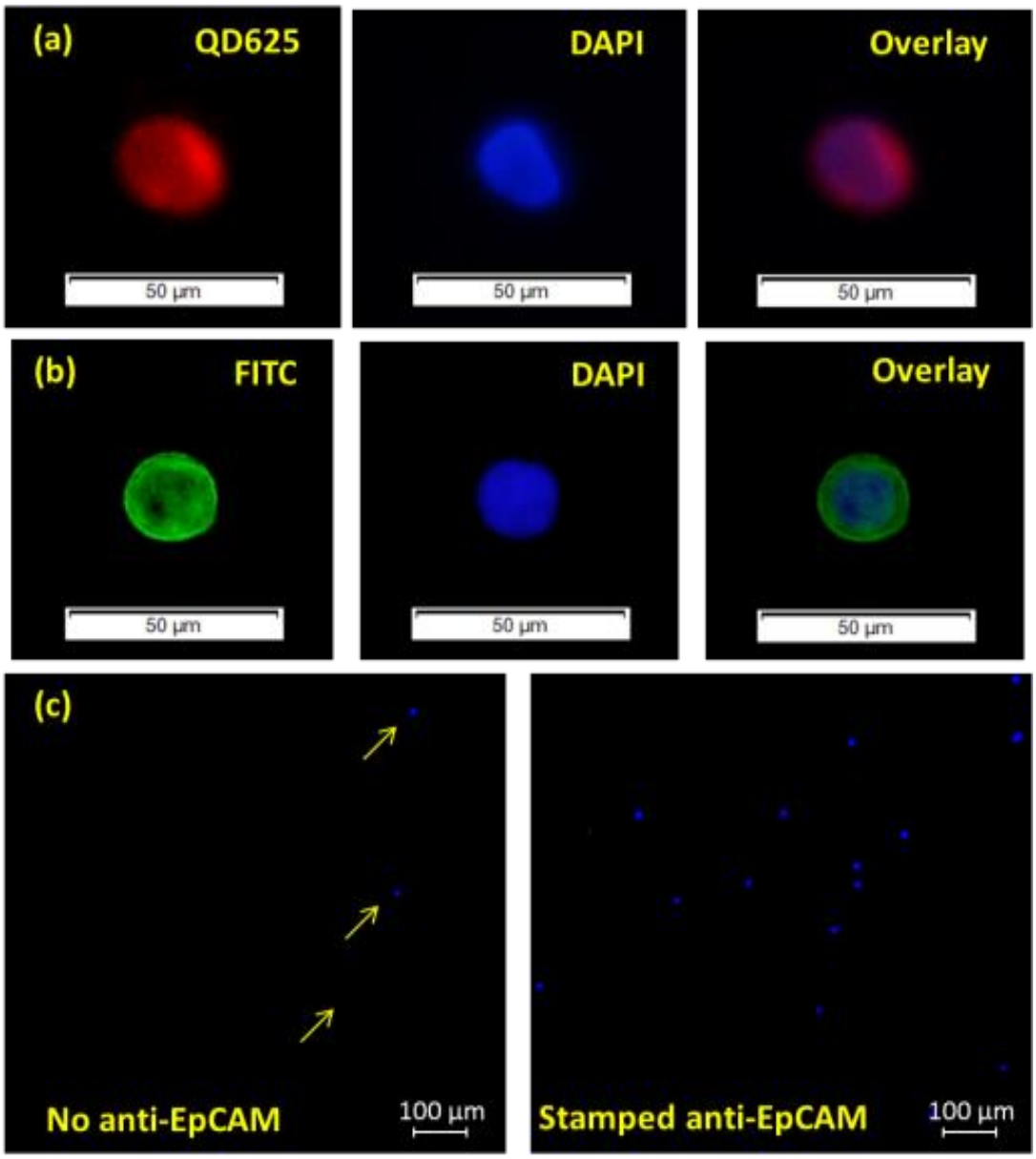

Figure 23. Cancer Cell Imaging. *Fluorescence microscopy images of captured SkBr3 cells and Colo205 cells on the nanoporous silica substrate. (a) The first row (left to right) images the SkBr3 cells' QD625-labeled HER2 surface receptors under a filter cube, DAPI stained nuclei under the DAPI filter, and an overlay of the DAPI and QD625 images. (b) The second row (left to right) images the Colo205 cell's FITC-labeled CK protein of the cytoskeleton under the FITC filter, DAPI stained nuclei under the DAPI filter, and an overlay of the DAPI and FITC images. (c) The third row (left to right) images the captured cell density within a defined area with no stamped anti-EpCAM, and the captured cell density within a defined area with stamped anti-EpCAM on the same nanoporous silica substrate.*

5.2.3 Statistical Analysis: Cancer Cell Capture Numbers

The number of captured cells for each experimental condition was counted within the defined 10 mm x 10 mm nanoporous silica square area for a total of five trials conducted under identical conditions. The average number of captured cells and respective standard deviations were obtained and the results are shown in **Table 2**.

Table 2. *Average captured cell numbers within the defined 1 cm x 1 cm nanoporous silica square area and respective standard deviations obtained from each of the six different experimental conditions.*

Cell Type	Condition	Stamped/No EpCAM Area	Average Capture Number per 25 mm^2 Area	Standard Deviation
SkBr3	1	Stamped EpCAM	55.50	23.18
	2	No EpCAM	13.10	9.79
Colo205	3	Stamped EpCAM	29.10	10.38
	4	No EpCAM	5.10	3.67
MDA-MB-435	5	Stamped EpCAM	2.00	1.63
	6	No EpCAM	3.25	2.87

Statistical analysis was performed to verify and compare the cancer cell capture numbers between the six different experimental conditions: 1) breast cancer cell line SkBr3 captured on microcontact printed anti-EpCAM nanoporous silica substrate, 2) SkBr3 captured on non-functionalized nanoporous silica substrate (negative control), 3) colon cancer cell line Colo205 captured on microcontact printed anti-EpCAM nanoporous silica substrate, 4) Colo205 captured on non-functionalized nanoporous silica substrate (negative control), 5) breast cancer cell line MDA-MB-435 captured on microcontact printed anti-EpCAM nanoporous silica substrate (negative control), and 6) MDA-MB-435 captured on non-functionalized nanoporous silica substrate (negative control). The one-way ANOVA test was used to calculate the *F* statistic, which in turn was used to determine the *p*-value. The *p*-value gives a measurement of how

statistically different the means of each experimental group are from each other. Here, a *p*-value of 0.05 is defined as the significance level. *P*-values greater than the significance level indicate that the means between experimental groups is not significantly different from each other. The opposite is true if *p*-values are equal to or less than the significance level. Further analysis using the Tukey's Method verified which specific two groups were statistically different from each other.

Table 3 shows the *p*-value for all group-by-group comparisons. Those outlined in green (*) (stamped EpCAM vs. non-stamped) and red (†) (experimental vs. control) indicate the major significant differences of importance that support the feasibility of the cell capture method. The one cell outlined in blue (‡) justifies the use of MDA-MB-435 cells as the negative control cell line.

Table 3. *Comparisons of all group-by-group p-values.*

		SkBr3	**Colo205**		**MDA-MB-435**	
		No EpCAM	Stamped EpCAM	No EpCAM	Stamped EpCAM	No EpCAM
SkBr3	Stamped EpCAM	4.589E-05*	4.000E-03	2.325E-06	1.606E-06†	1.734E-06†
	No EpCAM		2.800E-03	2.630E-02	1.050E-02	1.280E-02
Colo205	Stamped EpCAM			2.683E-06*	1.373E-06†	1.516E-06†
	No EpCAM				3.725E-01	4.857E-01
MDA-MB-435	Stamped EpCAM					8.260E-01‡

*Compares stamped vs. non-stamped EpCAM areas within each experimental cell lines
†Compares experimental cell lines vs. the negative control cell line
‡Compares stamped vs. non-stamped EpCAM areas within the negative control cell line

Table 2 shows a significant higher capture number between the number of SkBr3 cells captured on the stamped nanoporous silica area in comparison with the number of SkBr3 cells captured on non-stamped areas, indicating the feasibility of the method. The ANOVA test

comparing the two experimental conditions returned a *p*-value of 4.589E-5 (**Table 3**), thereby statistically justifying the feasibility of the method. The results of condition 1 are also significantly different from that of conditions 5 (MDA-MB-435, stamped EpCAM) and 6 (MDA-MB-435, no EpCAM), both of which served as negative controls, given MDA-MB-435 is an EpCAM negative cell line. This indicates that the SkBr3 cells were truly attracted to the stamped nanoporous silica surface mostly due to anti-EpCAM antibody-EpCAM antigen interactions and not simply adhering to the surface by means of other physical mechanisms.

Table 2 also shows a significant higher capture number between the number of Colo205 cells captured on the stamped nanoporous silica area in comparison with the number of Colo205 cells captured on non-stamped areas, again demonstrating the feasibility of the method. The ANOVA test comparing the two experimental conditions returned a *p*-value of 2.683E-6 (**Table 3**), again statistically justifying the feasibility of the method. Like condition 1 (SkBr3, stamped EpCAM), condition 3 (Colo205, stamped) also exhibited a significantly higher capture number in comparison to conditions 5 and 6. All results obtained from Tukey's Method were consistent with the group-by-group ANOVA comparisons shown in **Table 3**.

Variability in capture cell numbers across different cell lines can be attributed the biological differences between cell lines in biomarker expression. Various factors such as stage in cellular growth and development, cell health, and cell type contribute to the concentration and amount of expression of a particular biomarker on a cell's surface. Additional non-specific cell binding on the substrate surface may be due to the high density of cells used. In addition, physical contact between cells and surface and the porous nature of the silica thin film may serve to enhance mechanical attraction effects of cells to substrate. It has been shown that design alterations made to increase capture efficiencies can result in increase of non-specific binding as

well. As discussed in [77], this tradeoff is recognized and therefore balanced based on the intended device application, which in this case is the acquisition of targeted cells in specifically antibody defined locations, is made. Fluorescence immunoassay as a final step is also important and necessary to verify the detection and capture of the cell of interest, and can be seen used in other CTC screening chips that deal with complex samples and experience a number of non-specific bindings (white blood cells), as a supporting validation step [69, 70, 73].

5.3 Conclusion

In this section of the thesis, a method for the capture and detection of QD-labeled cancer cells on a surface was described. The system utilized the advantages of the spatially controlled large-scale patterning of microcontact printing and the enhanced absorption of antibodies of the nanoporous silica thin film substrates. The experiments described in the previous sections demonstrated proof of concept. Cancer cells were indeed successfully captured in areas of microcontact printed anti-EpCAM. Statistical analysis confirmed a significant difference between experimental and control conditions. It was also shown that the microchip has the specificity to differentiate EpCAM positive cells from EpCAM negative cells. This part of the thesis validated the capture of cancer cells within microcontact printed areas of antibodies in a static environment. This provides the foundation for the following part of the thesis, in which the microchip system is integrated with a microfluidic channel for enhanced site-specific targeted cancer cell capture.

6 Site-Specific Cancer Cell Detection in Microfluidics

This section of the thesis combines all the advantages of microcontact printed nanoporous silica substrates, QDs, with those of microfluidic channels into a wholesome integrated microchip-based cancer cell detection platform. With all elements combined, effective and efficient enhancement of the capture, detection, and imaging of cancer cells can be performed. This integration also uniquely allows for site-specific targeted cancer cell capture catered to particular microchannel geometries. Ultimately, such a platform can be designed to perform rare cell screening and detection for applications in cancer detection and diagnostics.

6.1 Experimental Methods

6.1.1 Microfluidic Modeling

To demonstrate microfluidic enhancement of cell capture, a design example was used. Here, a microfluidic channel of 20 mm long and 200 μm high was constructed with two grooves, each 5 mm wide, 100 μm deep, and spaced 3 mm apart from each other. The first groove was placed 1 mm away from the channel inlet. The inlet and outlet were modeled as two 50 μm wide by 200 μm high rectangles at the edges of the channel. A schematic of the microfluidic channel is shown in **Figure 24**.

The proposed grooved microchannel was modeled in COMSOL Multiphysics 4.2 to determine optimal locations for cell-surface interactions. Laminar flow at the walls was set to a no slip boundary condition. Flow at the inlet was set to a 0 Pa pressure and no viscous stress boundary condition. Flow at the outlet was set to a laminar outflow rate of 0.04 mL/s boundary condition. A free triangular mesh was constructed and scaled by a factor of 10 in the y-direction to capture more data points in the y-direction. The resulting velocity models were captured and

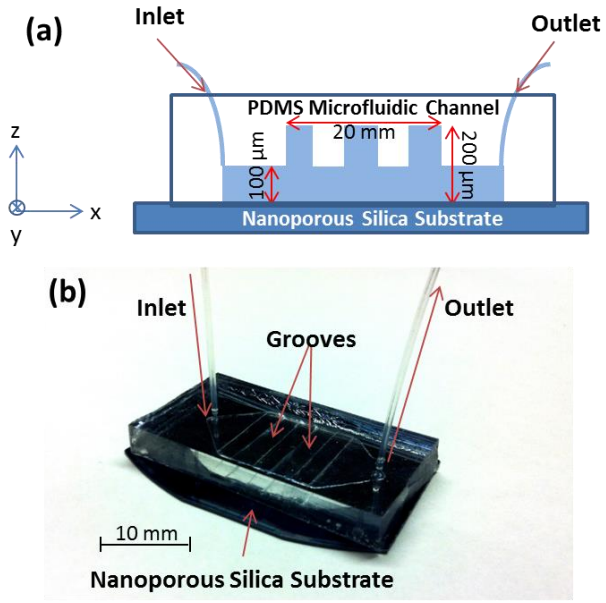

Figure 24. Model Microfluidic Channel. *(a) Side view of the grooved microfluidic channel and its dimensions. (b) Image of the grooved PDMS microchannel on nanoporous silica substrate with Teflon tubing for inlet and outlet.*

plotted for three solution sets: velocity magnitude, y-component velocity field, and x-component velocity field.

By determining optimal locations for cell-surface interactions within the microchannel through computer simulated models, controlled large-scale patterning of antibodies can be achieved for cancer cell capture at targeted specific areas on the substrate surface.

6.1.2 Site-Specific Cancer Cell Capture

A thin film plastic mold constructed from 100 µm thick plastic was used to create the grooved microchannels. The PDMS microchannels were fabricated in the same fashion as the PDMS stamps were fabricated, as described earlier (**Section 5.1.2**). Briefly, a PDMS mixture of 10:1 polymer to curing agent ratio was thoroughly mixed and desiccated. The mixture was then poured into the plastic mold and allowed to cure overnight.

Microfluidic experiments were then performed to demonstrate enhanced location-selective capture of cancer cells. Microcontact printing of anti-EpCAM was performed in a similar fashion as previously described in **Section 5.1.2**. Briefly, 2 mm x 4 mm rectangular PDMS stamps were incubated with anti-EpCAM, rinsed, dried, and then manually stamped onto the nanoporous silica surface at specific areas along the x-direction found in previously generated models (**Section 6.1.1**), as shown in **Figure 25**. After microcontact printing of anti-

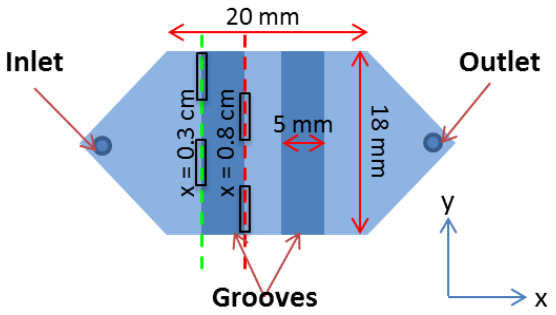

Figure 25. Site Specific Capture. *Top view of the grooved microfluidic channel and its dimensions. Optimal (green dashed lines) and non-optimal locations (red dashed lines) for cell-surface interaction based on COMSOL and MATLAB modeling results are shown. The black boxed areas indicate areas of microcontact printed anti-EpCAM antibodies.*

EpCAM, the prepared PDMS grooved microchannels were manually aligned and simply bonded directly onto the nanoporous silica substrate surface. Immuofluorescence detection of QD-labeled SkBr3 cancer cells was also performed in a similar fashion as previously described (**Section 5.2.2**). Briefly, a 3 mL SkBr3 cancer cell in PBS buffer solution (100,000 cells) was prepared and incubated with QD625-labeled anti-HER2 (50 µg/mL) and FITC-labeled anti-CK (20 µg/mL). Here, we use high cell densities to better illustrate the concept of being able to selectively capture cells in optimal areas while observing little to no binding of cells in non-optimal areas.

A syringe pump was used to draw liquid reagents and samples through the grooved microchannel at a flow rate of 2.5 mL/hr from a reservoir. A 1 mL 1% BSA (Sigma Aldrich) blocking solution was flowed into the microchannel and allowed to sit and incubate for 30 min. After the BSA blocking step, PBS (1 mL) was flowed in to rinse the channel and the FITC,QD625-labeled SkBr3 cancer cells were introduced into the channel. A final PBS rinse was then performed. To fix the captured cells onto the surface of the nanoporous substrate, 1 mL of glacial acetone was flowed into and incubated for 10 min in the channel as the channel was cooled in an ice bath. The PDMS microchannel was then peeled away from the substrate and the nanoporous substrate was placed under the microscope for fluorescence imaging after DAPI staining. The number of cells in each of the four test areas was counted along the *x*-direction (see coordinates in **Figure 25**) in a top to bottom fashion (along the negative *y*-direction).

6.1.3 Statistical Analysis

Statistical analysis was performed for the comparison of cell capture numbers between anti-EpCAM stamped optimal and nonoptimal areas on the substrate after integration of a grooved microfluidic channel. The averages and standard deviations were tabulated for each experiment's data set and the ANOVA test was used to make comparisons. For more detailed protocol, refer back to **Section 5.1.4**.

6.2 Results and Discussion

6.2.1 Modeling of the Microchannel

A microchannel 2 cm long and 200 μm high with grooves 5 mm wide and 100 μm deep was modeled. The resulting solution sets were plotted in COMSOL and MATLAB. Optimal locations along the length of the microchannel for cell-surface interactions were determined by plotting the y-component velocity field $0\ \mu m \leq y \leq 20\ \mu m$ (see **Figure 26**). This range of *y* values was chosen to be modeled in order to represent the streamline and velocity behavior of an average cancer cell (about 15 μm). Cells in this modeled range are more likely to be captured due to physical size and their relative *y*-position within the microchannel. Therefore, we are interested in studying the flow of single cells closest to the substrate surface. From the flow and velocity y-component profiles, the optimal location at which a single cell has highest probability of interacting with antibodies microcontact printed on the nanoporous silica substrate can be determined. Optimal locations can be defined by areas where the most negative V_y occurs, that is, at locations along the microchannel where the absolute minimum occurs. Alternatively, non-optimal locations are defined by areas where the most positive V_y, or the absolute maximum occurs. From the plot and data, it was found that three locations along the microchannel were

optimal for cell-surface interactions: 3469 μm, 11463 μm, and 19409 μm from the inlet. The three least optimal locations were also found: 566 μm, 8561 μm, and 16556 μm from the inlet.

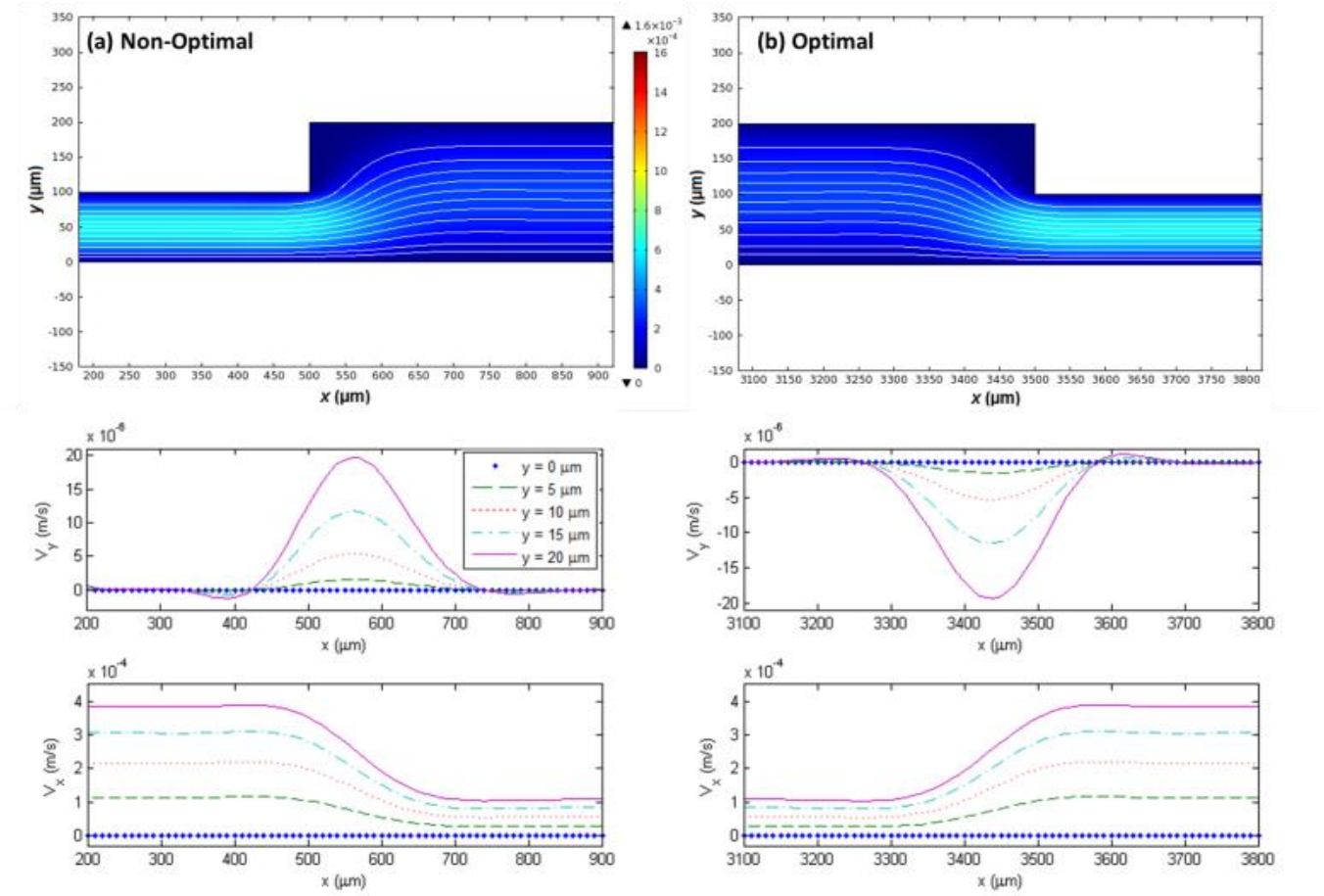

Figure 26. Microchannel Modeling. *The streamlines of flow as well as the theoretical x- and y- velocity fields at both (a) non-optimal and (b) optimal locations along the grooved microfluidic channel. The velocity components, V_x and V_y, were plotted for y-values of y = 0 μm (♦), 5 μm (--), 10 μm (··), 15 μm (–·), and 20 μm (—). Optimal locations along the microchannel occur where V_y is at absolute minimum and should be areas of highest probability for cell-surface interactions.*

Figure 26 shows an example of an optimal and a non-optimal location along the microchannel. The streamlines for flows at y = 0 μm, 5 μm, 10 μm, 15 μm, and 20 μm, as well as the corresponding V_y and V_x components are shown. It is understood that free flowing cells at heights y > 20 μm, may not experience a force large enough to allow interaction with capture antibodies and instead experience a slight dip in trajectory and continue its flow through the

channel. However, it can be seen in **Figure 26** that y = 20 μm, V_y is about 5% of V_x and decreases as y decreases. At optimal locations, a single cell traveling in the trajectories of the streamlines within the range 0 μm $\leq y \leq$ 20 μm, will have higher probability of interacting with capture antibodies at the surface of the nanoporous silica substrate than at non-optimal locations. This is because cells flowing through optimal locations, carried by fluid, will experience a larger downward velocity that generates a force which pushes the cell towards the capture antibodies stamped on the nanoporous silica surface.

6.2.2 Microfluidic Integration

To verify the feasibility of targeted spatial cancer cell capture, a grooved microfluidic channel was fabricated and integrated with a microcontact printed nanoporous silica substrate. As described earlier (**Section 6.1.2**), selected areas located at both optimal and non-optimal locations along the x-direction were stamped with anti-EpCAM. It is expected that areas with largest negative y-component velocity vector will observe higher cell capture than areas with largest positive y-component velocity vector. In addition, by controlling the spatial patterning of anti-EpCAM antibodies, we can further optimize cell capture capability by taking advantage of both the geometry of the microchannel and the microcontact printed antibodies.

From the microfluidic experiments, the number of captured SkBr3 cells within each anti-EpCAM stamped 2 mm x 4 mm nanoporous silica area was counted. It has been shown that current technologies for EpCAM based detection enables detection of rare cells down to about 5 cells/mL of blood [70]. Here, we use higher densities of cell numbers for experimental validation of the feasibility of our method and proof of concept. By using larger numbers of cells, we can better illustrate and emphasize the difference in numbers of cells selectively captured in optimal locations in comparison to the minimal number of cells captured in non-optimal locations.

It was found that the average number of cells captured in the expected optimal locations was 329.8 $\pm$ 32.3 cells. The average number of cells captured in the expected nonoptimal locations was 100 $\pm$ 12.6 cells. The ANOVA test returned a *p*-value of 1.130E-5, a value significantly less than 0.05, thereby statistically justifying the feasibility of the method and the cell capture enhancement through integration of a grooved microfluidic channel on an antibody-patterned nanoporous silica substrate. **Figure 27** contrasts the captured cell density within an anti-EpCAM stamped area in an optimal location along the microchannel with the captured cell density within an anti-EpCAM stamped area in a nonoptimal location along the microchannel on the nanoporous silica substrate. It can be seen that the captured cell density within the expected optimal area is higher than that within the expected nonoptimal area.

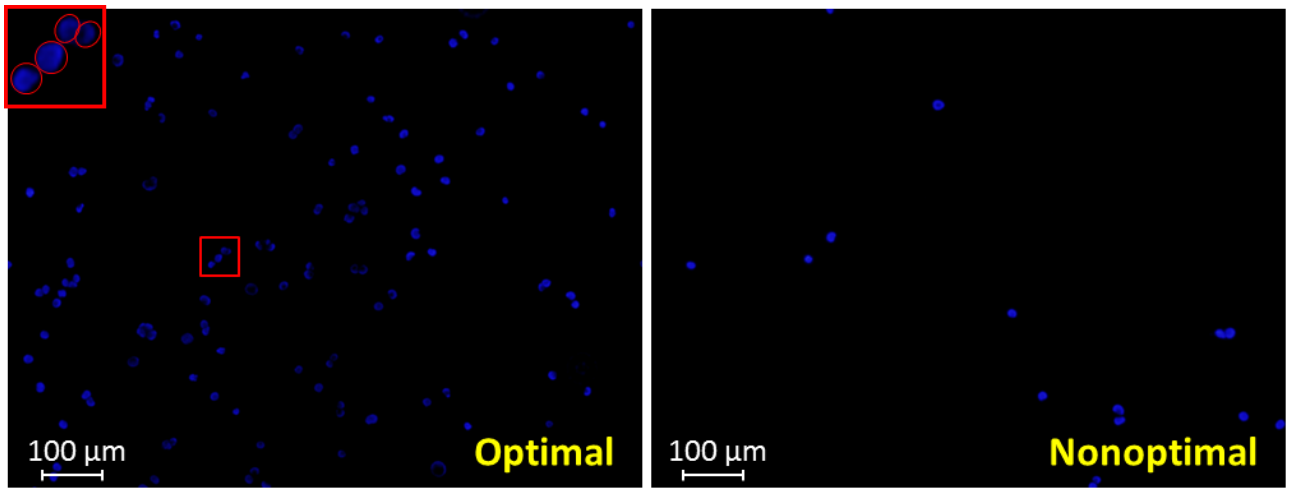

Figure 27. ***Capture Site-Specific Cancer Cell Imaging.*** *Fluorescence microscopy images of captured SkBr3 cells on the nanoporous silica substrate from microfluidic experiments. The DAPI images show the captured cell density within a stamped anti-EpCAM area of an optimal location along the microchannel and the captured cell density within a stamped anti-EpCAM area of a nonoptimal location along the microchannel on the same nanoporous silica substrate.*

6.3 Conclusion

In this section of the thesis, a method for site specific capture and detection of QD-labeled cancer cells within a static environment was described. The system utilized the advantages of the spatially controlled patterning of microcontact printing and the enhanced absorption of antibodies of the nanoporous silica thin film substrates. Most importantly, the system also utilized the advantage of a microfluidic channel to increase the probability of cell-surface interactions. By confining the reagent and sample fluids to a microscale volume within a grooved microchannel, a micromixing environment was created and further enhanced the chance of binding between the microcontact printed anti-EpCAM on the nanoporous silica substrate and the EpCAM biomarkers on the cancer cells' surface. The experiments described in the previous sections demonstrated proof of concept. Cancer cells were indeed successfully captured in areas of microcontact printed anti-EpCAM. Statistical analysis confirmed a significant difference between experimental and control conditions. This part of the thesis validated the capture of cancer cells within specifically defined microcontact printed optimal locations within a grooved microfluidic channel.

It can therefore be seen that the integration of the following micro and nanotechnologies and techniques into an integrated microchip-based platform can create an effective and efficient system for cancer diagnostics and detection: 1) microcontact printing, 2) nanoporous silica thin film substrate, 3) quantum dots, and 3) microfluidic channels. This platform can be further developed into a detection system for rare cell detection, especially for CTC detection in whole blood. Combined, the technologies allow for specific and selective capture of cancer cells that incorporate the additional low cost and high throughput advantages of micro and nanotechnologies.

7 Closing Remarks and Future Directions

This thesis presents a description of the design and experimental pathway that was undertaken to develop a method for the capture and detection of QD-labeled cancer cells in microfluidic chips. Efficient cell capture was achieved on a site-specific microcontact printed nanoporous silica substrate via antibody-antigen interactions within a grooved microfluidic channel. The method of capture and detection utilizes and optimizes the advantages of four components: 1) microcontact printing for quick, easy, and efficient transfer of proteins or antibodies, 2) nanoporous silica thin film substrate for enhanced protein absorption and surface functionalization, 3) quantum dots for brighter and more stable imaging, and 4) site-specific capture sites unique to microfluidic channel geometries to enhance the cell-surface interaction at predetermined optimal areas.

Potential applications for such a system includes high throughput screening, drug assays and *in vivo* diagnostics, site-specific cell culturing, as well as cancer cell biomarker studies. The flexibility to spatially define capture sites at optimal locations, in combination with single chip integration, microfluidics and QD-labeling, enables further multiplexing and multicolor detection capabilities. Multiple cancer cell lines would be able to be detected on the same substrate and multicolor labeled biomarkers can be simultaneously detected in such integrated micro total analysis systems. As seen throughout this thesis, the integrated platforms show great promise for a broad range of biomedical applications.

8 References

[1] "What Is Cancer?," *American Cancer Society*, 2012. [Online]. Available: http://www.cancer.org/Cancer/CancerBasics/what-is-cancer. [Accessed: 06-Aug-2012].

[2] "What Causes Cancer?," *American Cancer Society*, 2012. [Online]. Available: http://www.cancer.org/Cancer/CancerCauses/index. [Accessed: 06-Aug-2012].

[3] "WHO | Cancer," *WHO*. [Online]. Available: http://www.who.int/mediacentre/factsheets/fs297/en/. [Accessed: 06-Aug-2012].

[4] B. Mostert, S. Sleijfer, J. A. Foekens, and J. W. Gratama, "Circulating tumor cells (CTCs): Detection methods and their clinical relevance in breast cancer," *Cancer Treatment Reviews*, vol. 35, no. 5, pp. 463-474, Aug. 2009.

[5] "Circulating tumor cells can provide 'real-time' information on patient's current disease state," *ScienceDaily*. [Online]. Available: http://www.sciencedaily.com/releases/2010/09/100928135039.htm. [Accessed: 06-Aug-2012].

[6] R.C. Bast, H. Lilja, N. Urban, D.L. Rimm, H. Fritsche, J. Gray, R. Veltri, G. Klee, A. Allen, N. Kim, S. Gutman, M. Rubin, A. Hruszkewycz. "Translational Crossroads for Biomarkers," *Clinical Cancer Research*, vol. 11, no. 17, pp. 6103-6108, Sep. 2005.

[7] S. Menard, S. Fortis, F. Castiglioni, R. Agresti, and A. Balsari, "HER2 as a Prognostic Factor in Breast Cancer," *Oncology*, vol. 61, no. 2, pp. 67-72, 2001.

[8] C. Sotiriou and L. Pusztai, "Gene-Expression Signatures in Breast Cancer," *N Engl J Med*, vol. 360, no. 8, pp. 790-800, 2009.

[9] "Veridex, LLC, a Johnson & Johnson company in vitro diagnostics oncology." [Online]. Available: http://www.veridex.com/CellSearch/Patients/CellSearchCTC.aspx. [Accessed: 07-Aug-2012].

[10] C. for D. and R. Health, "Recently-Approved Devices - CellSearch™ Epithelial Cell Kit / CellSpotter™ Analyzer - K031588." [Online]. Available: http://www.fda.gov/MedicalDevices/ProductsandMedicalProcedures/DeviceApprovalsandClearances/Recently-ApprovedDevices/ucm081239.htm. [Accessed: 07-Aug-2012].

[11] E.A. Punnoose, S.K. Atwal, J.M. Spoerke, H. Savage, A. Pandita, R. Yeh, A. Pirzkall, B.M. Fine, L.C. Amler, D.S. Chen, M.R. Lackner. "Molecular Biomarker Analyses Using Circulating Tumor Cells," 2010.

[12] S. Mousa, "Biosensors: the new wave in cancer diagnosis," *Nanotechnology, Science and Applications*, p. 1, Dec. 2010.

[13] Y. Ikada, "Surface modification of polymers for medical applications," *Biomaterials*, vol. 15, no. 10, pp. 725-736, Aug. 1994.

[14] C.-M. Chan, T.-M. Ko, and H. Hiraoka, "Polymer surface modification by plasmas and photons," *Surface Science Reports*, vol. 24, no. 1–2, pp. 1-54, May 1996.

[15] A.S. Maria Chong and X.S. Zhao, "Functionalization of SBA-15 with APTES and Characterization of Functionalized Materials," *J. Phys. Chem. B*, vol. 107, no. 46, pp. 12650-12657, 2003.

[16] G.L. Kenausis, J. Vörös, D.L. Elbert, N. Huang, R. Hofer, L. Ruiz-Tayler, M. Textor, J.A. Hubbell, N.D. Spencer, "Poly(l-lysine)-g-Poly(ethylene glycol) Layers on Metal Oxide Surfaces: Attachment Mechanism and Effects of Polymer Architecture on Resistance to Protein Adsorption†," *J. Phys. Chem. B*, vol. 104, no. 14, pp. 3298-3309, 2000.

[17] E. Blinka, K. Loeffler, Y. Hu, A. Gopal, K. Hoshino, K. Lin, X. Liu, M. Ferrari, X.J. Zhang, "Enhanced Microcontact Printing of Proteins on Nanoporous Silica Surface," *Nanotechnology*, vol. 21, no. 41, p. 415302, Oct. 2010.
[18] Y. Hu, A. Bouamrani, E. Tasciotti, L. Li, X. Liu, and M. Ferrari, "Tailoring of the Nanotexture of Mesoporous Silica Films and Their Functionalized Derivatives for Selectively Harvesting Low Molecular Weight Protein," *ACS Nano*, vol. 4, no. 1, pp. 439-451, 2009.
[19] T.A. Desai, D.J. Hansford, L. Leoni, M. Essenpreis, and M. Ferrari, "Nanoporous anti-fouling silicon membranes for biosensor applications," *Biosensors and Bioelectronics*, vol. 15, no. 9–10, pp. 453-462, Nov. 2000.
[20] T.A. Desai, D.J. Hansford, L. Kulinsky, A.H. Nashat, G. Rasi, J. Tu, Y. Wang, M. Zhang, and M. Ferrari, "Nanopore Technology for Biomedical Applications," *Biomedical Microdevices*, vol. 2, no. 1, pp. 11-40, Feb. 1999.
[21] P. Somasundaran, *Encyclopedia of Surface And Colloid Science*. CRC Press, 2006.
[22] J.L. Wilbur, A. Kumar, H.A. Biebuyck, E. Kim, and G.M. Whitesides, "Microcontact printing of self-assembled monolayers: applications in microfabrication," *Nanotechnology*, vol. 7, no. 4, pp. 452-457, Dec. 1996.
[23] M. Mrksich and G.M. Whitesides, "Patterning self-assembled monolayers using microcontact printing: A new technology for biosensors?," *Trends in Biotechnology*, vol. 13, no. 6, pp. 228-235, Jun. 1995.
[24] E. Ng, A. Gopal, K. Hoshino, and X. Zhang, "Multicolor microcontact printing of proteins on nanoporous surface for patterned immunoassay," *Applied Nanoscience*, vol. 1, no. 2, pp. 79-85, Apr. 2011.
[25] H.D. Inerowicz, S. Howell, F.E. Regnier, and R. Reifenberger, "Multiprotein Immunoassay Arrays Fabricated by Microcontact Printing," *Langmuir*, vol. 18, no. 13, pp. 5263-5268, 2002.
[26] J. Lahiri, E. Ostuni, and G.M. Whitesides, "Patterning Ligands on Reactive SAMs by Microcontact Printing," *Langmuir*, vol. 15, no. 6, pp. 2055-2060, 1999.
[27] J.P. Renault, A. Bernard, A. Bietsch, B. Michel, H.R. Bosshard, E. Delamarche, M. Kreiter, B. Hecht, U.P. Wild, "Fabricating Arrays of Single Protein Molecules on Glass Using Microcontact Printing," *J. Phys. Chem. B*, vol. 107, no. 3, pp. 703-711, 2002.
[28] A. Bernard, E. Delamarche, H. Schmid, B. Michel, H.R. Bosshard, and H. Biebuyck, "Printing Patterns of Proteins," *Langmuir*, vol. 14, no. 9, pp. 2225-2229, 1998.
[29] D.F. Williams, *The Biomaterials Silver Jubilee Compendium: The Best Papers Published in Biomaterials, 1980-2004*. Elsevier, 2007.
[30] D.C. Turner, C. Chang, K. Fang, S.L. Brandow, and D.B. Murphy, "Selective adhesion of functional microtubules to patterned silane surfaces.," *Biophysical Journal*, vol. 69, no. 6, pp. 2782-2789, Dec. 1995.
[31] M. Mrksich, L E. Dike, J. Tien, D.E. Ingber, and G.M. Whitesides, "Using microcontact printing to pattern the attachment of mammalian cells to self-assembled monolayers of alkanethiolates on transparent films of gold and silver," *Experimental cell research*, vol. 235, no. 2, pp. 305-313, Sep. 1997.
[32] C.D. James, R. Davis, M. Meyer, A. Turner, S. Turner, G. Withers, L. Kam, G. Banker, H. Craighead, M. Issacson, J. Turner, W. Shain, "Aligned microcontact printing of micrometer-scale poly-L-Lysine structures for controlled growth of cultured neurons on

planar microelectrode arrays," *IEEE Transactions on Biomedical Engineering*, vol. 47, no. 1, pp. 17-21, Jan. 2000.
[33] A. Gopal, K. Hoshino, S. Kim, and X. Zhang, "Multi-color colloidal quantum dot based light emitting diodes micropatterned on silicon hole transporting layers," *Nanotechnology*, vol. 20, no. 23, p. 235201, Jun. 2009.
[34] V. Santhanam and R.P. Andres, "Microcontact Printing of Uniform Nanoparticle Arrays," *Nano Lett.*, vol. 4, no. 1, pp. 41-44, 2003.
[35] A. Rizzo, M. Mazzeo, M. Palumbo, G. Lerario, S. D'Amone, R. Cingolani. G. Gigli, "Hybrid Light-Emitting Diodes from Microcontact-Printing Double-Transfer of Colloidal Semiconductor CdSe/ZnS Quantum Dots onto Organic Layers," *Advanced Materials*, vol. 20, no. 10, pp. 1886-1891, 2008.
[36] H. Schmid and B. Michel, "Siloxane Polymers for High-Resolution, High-Accuracy Soft Lithography," *Macromolecules*, vol. 33, no. 8, pp. 3042-3049, 2000.
[37] Y. Li, C. Song, K. Zhang, M. Wang, K. Yang, A. Yang, B. Jin, "Establishment of a Highly Sensitive Sandwich Enzyme-Linked Immunosorbent Assay Specific for Ovomucoid from Hen's Egg White," *Journal of Agricultural and Food Chemistry*, vol. 56, no. 2, pp. 337-342, Jan. 2008.
[38] J.R. Crowther, *The ELISA Guidebook - Second Edition*. 2009.
[39] J.M. Rolland, E. Apostolou, M.P. de Leon, C.S. Stockley, and R.E. O'Hehir, "Specific and Sensitive Enzyme-Linked Immunosorbent Assays for Analysis of Residual Allergenic Food Proteins in Commercial Bottled Wine Fined with Egg White, Milk, and Nongrape-Derived Tannins," *J. Agric. Food Chem.*, vol. 56, no. 2, pp. 349-354, 2007.
[40] O. Stephan and S. Vieths, "Development of a Real-Time PCR and a Sandwich ELISA for Detection of Potentially Allergenic Trace Amounts of Peanut (Arachis hypogaea) in Processed Foods," *J. Agric. Food Chem.*, vol. 52, no. 12, pp. 3754-3760, 2004.
[41] J. Sun, "Development of enzyme linked immunoassay for the simultaneous detection of carbaryl and metolcarb in different agricultural products," *Analytica Chimica Acta*, vol. 666, no. 1-2, pp. 76-82, May 2010.
[42] O. Manasreh, *Introduction to Nanomaterials and Devices*, 1st ed. Chicester: Wiley, 2011.
[43] V. I. Klimov, *Nanocrystal Quantum Dots*, 2nd ed. Hoboken: CRC Press, 2010.
[44] B. Valeur and M.N. Berberan-Santos, *Molecular Fluorescence : Principles and Applications*, 2nd ed. Weinheim: Wiley, 2013.
[45] P. Reinke, *Inorganic Nanostructures : Properties and Characterization*, 1st ed. Weinheim: Wiley, 2012.
[46] I.L. Medintz, H.T. Uyeda, E.R. Goldman, and H. Mattoussi, "Quantum dot bioconjugates for imaging, labelling and sensing," *Nat Mater*, vol. 4, no. 6, pp. 435-446, Jun. 2005.
[47] M. Nichkova, D. Dosev, A.E. Davies, S.J. Gee, I.M. Kennedy, and B.D. Hammock, "Quantum Dots as Reporters in Multiplexed Immunoassays for Biomarkers of Exposure to Agrochemicals," *Analytical Letters*, vol. 40, no. 7, pp. 1423-1433, 2007.
[48] X. Michalet et al., "Quantum Dots for Live Cells, in vivo Imaging, and Diagnostics," *Science*, vol. 307, no. 5709, pp. 538-544, Jan. 2005.
[49] X. Wu, H. Liu, J. Liu, K. Haley, J.A. Treadway, J.P. Larson, N. Ge, F. Peale, M.P. Bruchez, "Immunofluorescent labeling of cancer marker Her2 and other cellular targets with semiconductor quantum dots," *Nat Biotech*, vol. 21, no. 1, pp. 41-46, Jan. 2003.

[50] X. Gao, Y. Cui, R.M. Levenson, L.W.K. Chung, and S. Nie, "In vivo: cancer targeting and imaging with semiconductor quantum dots : Abstract : Nature Biotechnology," *Nature Biotechnology*, vol. 22, no. 8, pp. 969-976, Jul. 2004.
[51] R. Brayner, F. Fiévet, and T. Coradin, *Nanomaterials: A Danger or a Promise?*, 1st ed. Dordrecht: Springer, 2012.
[52] J.W. Uhr, M. Huebschman, E.P. Frenkel, N.L. Lane, R. Ashfaq, H. Liu, D.R. Rana, L. Cheng, A.T. Lin, G.A. Hughes, X.J. Zhang, H.R. Garner, "Molecular profiling of individual tumor cells by hyperspectral microscopic imaging," *Translational research: the journal of laboratory and clinical medicine*, vol. 159, no. 5, pp. 366-375, May 2012.
[53] W.K. Bae, J.H. Lim, D.G. Lee, M.K. Nam, K.H. Char, C.H. Lee, S.H. Lee, "Multicolored Light-Emitting Diodes Based on All-Quantum-Dot Multilayer Films Using Layer-by-Layer Assembly Method," *Nano Lett.*, vol. 10, no. 7, pp. 2368-2373, 2010.
[54] F. Maier-Flaig, J. Rinck, M. Stephan, T. Bocksrocker, M. Bruns, C. Kübel, A.K. Powell, G.A Ozin, U. Lemmer, "Multicolor Silicon Light-Emitting Diodes (SiLEDs)," *Nano Lett.*, vol. 13, no. 2, pp. 475-480, 2013.
[55] A. Gopal, "Multicolor Colloidal Quantum Dot Based Inorganic Light Emitting Diode on Silicon: Design, Fabrication and Biomedical Applications," The University of Texas at Austin, Austin, Texas, December 2011.
[56] J. Khandurina, T.E. McKnight, S.C. Jacobson, L.C. Waters, R.S. Foote, and J.M. Ramsey, "Integrated System for Rapid PCR-Based DNA Analysis in Microfluidic Devices," *Anal. Chem.*, vol. 72, no. 13, pp. 2995-3000, 2000.
[57] E.T. Lagally, I. Medintz, and R.A. Mathies, "Single-Molecule DNA Amplification and Analysis in an Integrated Microfluidic Device," *Anal. Chem.*, vol. 73, no. 3, pp. 565-570, 2001.
[58] E.T. Lagally, P.C. Simpson, and R.A. Mathies, "Monolithic integrated microfluidic DNA amplification and capillary electrophoresis analysis system," *Sensors and Actuators B: Chemical*, vol. 63, no. 3, pp. 138-146, May 2000.
[59] M.A. McClain, C.T. Culbertson, SC. Jacobson, and J.M. Ramsey, "Flow Cytometry of Escherichia coli on Microfluidic Devices," *Anal. Chem.*, vol. 73, no. 21, pp. 5334-5338, 2001.
[60] L. Wang, L.A. Flanagan, N.L. Jeon, E. Monuki, and A.P. Lee, "Dielectrophoresis switching with vertical sidewall electrodes for microfluidic flow cytometry," *Lab Chip*, vol. 7, no. 9, pp. 1114-1120, 2007.
[61] J. Godin, C.H. Chen, S.H. Cho, W. Qiao, F. Tsai, and Y.H. Lo, "Microfluidics and photonics for Bio-System-on-a-Chip: A review of advancements in technology towards a microfluidic flow cytometry chip," *Journal of Biophotonics*, vol. 1, no. 5, pp. 355-376, 2008.
[62] A.E. Herr, A.V. Hatch, D. Throckmorton, H.M. Tran, J.S. Brennan, W. Giannobile, A.K. Singh, "Microfluidic immunoassays as rapid saliva-based clinical diagnostics," *Proceedings of the National Academy of Sciences*, vol. 104, no. 13, pp. 5268-5273, Mar. 2007.
[63] J. Yakovleva, R. Davidsson, A. Lobanova, M. Bengtsson, S. Eremin, T. Laurell, J. Emnéus, "Microfluidic Enzyme Immunoassay Using Silicon Microchip with Immobilized Antibodies and Chemiluminescence Detection," *Analytical Chemistry*, vol. 74, no. 13, pp. 2994-3004, Jul. 2002.

[64] A. Bange, H.B. Halsall, and W.R. Heineman, "Microfluidic immunosensor systems," *Biosensors and Bioelectronics*, vol. 20, no. 12, pp. 2488-2503, Jun. 2005.
[65] F.B. Myers and L.P. Lee, "Innovations in optical microfluidic technologies for point-of-care diagnostics," *Lab Chip*, vol. 8, no. 12, pp. 2015-2031, 2008.
[66] H.A. Stone and S. Kim, "Microfluidics: Basic issues, applications, and challenges," *AIChE Journal*, vol. 47, no. 6, pp. 1250-1254, 2000.
[67] C. Hansen and S. R. Quake, "Microfluidics in structural biology: smaller, faster… better," *Current Opinion in Structural Biology*, vol. 13, no. 5, pp. 538-544, Oct. 2003.
[68] J.R. Anderson, D.T. Chiu, H. Wu, O.J. Schueller, and G.M. Whitesides, "Fabrication of microfluidic systems in poly (dimethylsiloxane)," *Electrophoresis*, vol. 21, pp. 27-40, 2000.
[69] K. Hoshino, Y.Y. Huang, N. Lane, M. Huebschman, J.W. Uhr, E.P. Frenkel, X.J. Zhang, "Microchip-based immunomagnetic detection of circulating tumor cells," *Lab Chip*, vol. 11, no. 20, pp. 3449-3457, Aug. 2011.
[70] S.L. Stott, C.H. Hsu, D.I. Tsukrov, M. Yu, D.T. Miyamoto, B.A. Waltman, S.M. Rothenberg, A.M. shah, M.E. Smas, G.K. Korir, F.P. Floyd, A.J. Gilman, J.B. Lord, D. Winokur, S. Springer, D. Irimia, S. Nagrath, L.V. Sequist, R.J. Lee, K.J. Isselbacher, S. Maheswaran, D.A. Haber, M. Toner, "Isolation of circulating tumor cells using a microvortex-generating herringbone-chip," *Proceedings of the National Academy of Sciences*, vol. 107, no. 43, pp. 18392-18397, Oct. 2010.
[71] T.P. Forbes and J.G. Kralj, "Engineering and analysis of surface interactions in a microfluidic herringbone micromixer," *Lab on a Chip*, vol. 12, no. 15, pp. 2634-2637, 2012.
[72] N.S. Lynn and D.S. Dandy, "Geometrical optimization of helical flow in grooved micromixers," *Lab Chip*, vol. 7, no. 5, pp. 580-587, 2007.
[73] S. Nagrath, L.V. Sequist, S. Maheswaran, D.W, Bell, D. Irimia, L. Ulkus, M.R. Smith, E.L. Kwak, S. Digumarthy, A. Muzikansky, P. Ryan, U.J. Balis, R.G. Tompkins, D.A. Haber, M. Toner, "Isolation of rare circulating tumour cells in cancer patients by microchip technology," *Nature*, vol. 450, no. 7173, pp. 1235-1239, Dec. 2007.
[74] D. Huh, B.D. Matthews, A. Mammoto, M. Montoya-Zavala, H.Y. Hsin, and D.E. Ingber, "Reconstituting Organ-Level Lung Functions on a Chip," *Science*, vol. 328, no. 5986, pp. 1662 -1668, Jun. 2010.
[75] D. Huh, D.C. Leslie, B. Matthews, J.P. Fraser, S. Jurek, G. Hamilton, K.S. Thorneloe, M. McAlexander, D.E. Ingber, "A Human Disease Model of Drug Toxicity–Induced Pulmonary Edema in a Lung-on-a-Chip Microdevice," *Science Translational Medicine*, vol. 4, no. 159, p. 159ra147, Nov. 2012.
[76] L. Wu, D. Carlo, and L. Lee, "Microfluidic self-assembly of tumor spheroids for anticancer drug discovery," *Biomedical Microdevices*, vol. 10, no. 2, pp. 197-202, 2008.
[77] P. Li, Z. S. Stratton, M. Dao, J. Ritz, and T. J. Huang, "Probing circulating tumor cells in microfluidics," *Lab Chip*, vol. 13, no. 4, pp. 602-609.